How the rock-inhabiting fungus K. petricola A95 enhances olivine dissolution through attachment

R Gerrits, R Pokharel, R. Breitenbach, J. Radnik, I Feldmann, J Schuessler, F von Blanckenburg, A.A. Gorbushina, J. Schott

Available online at www.sciencedirect.com

ScienceDirect

Geochimica et Cosmochimica Acta 282 (2020) 76–97

Geochimica et Cosmochimica Acta

www.elsevier.com/locate/gca

How the rock-inhabiting fungus *K. petricola* A95 enhances olivine dissolution through attachment

R. Gerrits [a], R. Pokharel [b,c], R. Breitenbach [a], J. Radnik [d], I. Feldmann [a], J.A. Schuessler [b,e], F. von Blanckenburg [b,g], A.A. Gorbushina [a,f,g,*], J. Schott [h]

[a] *Bundesanstalt für Materialforschung und -prüfung (BAM), Department 4, Material und Umwelt, 12205 Berlin, Germany*
[b] *GFZ German Research Centre for Geosciences, Earth Surface Geochemistry, 14473 Potsdam, Germany*
[c] *Université de Rennes, Ecole Nationale Superieure de Chimie de Rennes, 35000 Rennes, France*[1]
[d] *Bundesanstalt für Materialforschung und -prüfung (BAM), Department 6, Materialchemie, 12205 Berlin, Germany*
[e] *Thermo Fisher Scientific, 28199 Bremen, Germany*[2]
[f] *Freie Universität Berlin, Fachbereich Biologie, Chemie und Pharmazie, 14195 Berlin, Germany*
[g] *Freie Universität Berlin, Fachbereich Geowissenschaften, 12249 Berlin, Germany*
[h] *Université de Toulouse CNRS, Géosciences Environnement Toulouse (GET), Observatoire Midi-Pyrénées, 31400 Toulouse, France*

Received 21 January 2020; accepted in revised form 7 May 2020; available online 16 May 2020

Abstract

Free-living and mycorrhizal fungi are able to enhance the weathering of rock and other solid substrates. Deciphering the exact mechanisms of these natural processes requires their experimental simulation. Moreover, by performing these simulations with genetically amenable rock-weathering fungi, one can knock-out certain fungal traits and consequently identify their weathering-relevant function. Here, the effect of the rock-inhabiting fungus, *Knufia petricola* A95, on the dissolution kinetics of an Fe-bearing olivine ($Mg_{1.86}Fe_{0.19}SiO_4$) is investigated at 25 °C and pH 6 using reproducible batch and mixed flow experiments. The availability of a melanin-deficient mutant (Δ*Kppks*) of *K. petricola* A95, which produces more extracellular polymeric substances (EPS) than the wild type (WT), enables the comparative study of the role of melanin and EPS in olivine dissolution. In abiotic dissolution experiments, the olivine dissolution rate decreased considerably over time at pH 6 but not at pH 3.5. This inhibition of abiotic olivine dissolution at pH 6 was most likely caused by the *in-situ* oxidation of ferrous Fe and/or the precipitation of ferric hydroxides at the olivine surface. In corresponding biotic experiments at pH 6, both the wild type *K. petricola* and its melanin-deficient mutant Δ*Kppks* solubilised and bound significant amounts of Fe released by olivine dissolution. Fe oxidation and precipitation were thus prevented and olivine dissolution proceeded faster than in the abiotic experiments. By sequestering Fe directly at the olivine surface, the attached wild type *K. petricola* cells were particularly efficient at preventing the oxidation of Fe at the mineral surface: the slowdown of olivine dissolution almost completely disappeared. The attachment capacity of these wild type cells is most likely mediated by wild type-specific EPS. Our presented experimental systems allow the oxidation of mineral-released Fe and include a rock-inhabiting fungus, thus simulating chemical, physical and biological conditions that set dissolution rates in a way that is relevant to natural ecosystems.

Keywords: Bio-weathering; Forsterite; Knock-out mutant; Extracellular polymeric substances; Melanin; Adhesion; Black fungi

* Corresponding author at: Bundesanstalt für Materialforschung und -prüfung (BAM), Abteilung 4, Material und Umwelt, 12205 Berlin, Germany.
E-mail address: anna.gorbushina@bam.de (A.A. Gorbushina).
[1] Present address.
[2] Present address.

https://doi.org/10.1016/j.gca.2020.05.010
0016-7037/

1. INTRODUCTION

The involvement of fungi and lichens in rock weathering processes at the Earth's surface has been documented in numerous studies (Ahmadjian and Hale, 1973; Krumbein and Jens, 1981; Banfield et al., 1999; Adeyemi and Gadd, 2005; Bonneville et al., 2009; Cai et al., 2013). However, the exact mechanisms of fungi-induced weathering are less known (Hoffland et al., 2004). In general, these can be divided into two groups: biochemical and biomechanical mechanisms (Gadd, 2007). The former involves the excretion of metal-complexing compounds (e.g. phenols, acids or Fe-binding siderophores), the reduction of the pH and the production of enzymes like ferric reductases (Drever and Stillings, 1997; Vartivarian and Cowart, 1999; Abdulla, 2009). The latter entails processes like the penetration of hyphae into minerals, the encapsulation of grains by the cellular aggregates (i.e. the biofilm) and the splitting of minerals through water ad- and desorption by their extracellular polymeric substances (EPS) (Duane, 2006; Bonneville et al., 2016).

Our study focusses on fungal traits, relevant to mineral weathering, which are located at the cell surface, where direct contact with the mineral probably occurs. In this study we therefore address the production of melanin and EPS, present at the outer layers of the fungal cell wall. Melanin is a macromolecular black-brownish, phenol-containing, humic acid-like pigment that can be found in or around the cell wall of plant, animal, bacterial and fungal cells (Fogarty and Tobin, 1996). Its unique properties not only make fungal cells more resistant to various environmental stresses (Fogarty and Tobin, 1996; Gorbushina, 2007; Paolo et al., 2006), they also impact weathering. For instance, the ability of pure melanin to selectively bind metals enables the higher metal binding capacity of melanised fungal cells (Gadd and Derome, 1988; Siegel et al., 1990), protecting against metal toxicity and possibly driving weathering. Furthermore, melanin's ability to reduce the cell wall permeability (Howard and Ferrari, 1989; Howard et al., 1991) might enable the fungal cell to maintain turgor pressure during water stress (Fernandez and Koide, 2013) and to reach the pressures required to penetrate a substrate (Howard et al., 1991; Money and Howard, 1996). A melanised appressorium is able to reach an elastic modulus in the range of 10–100 MPa (Goriely and Tabor, 2006), which according to Li et al. (2016) would be sufficient to break down silicate minerals.

Microbial growth on surfaces (i.e. a biofilm) is characterised by the formation of EPS (Flemming et al., 2016). EPS consists of a mixture of polysaccharides, proteins, lipids and extracellular DNA (Flemming et al., 2016). It forms a polymer layer around the cells, provides protection against antibiotics and desiccation, and traps nutrients (Flemming et al., 2016; Gorbushina, 2007). EPS can accelerate or inhibit mineral dissolution (Tourney and Ngwenya, 2014). The accelerating effect is mostly caused by the binding of metals to EPS, the presence of organic acids and enzymes in the EPS structure, and the pressure exerted on the mineral surface by repeated wetting and drying cycles (Warscheid and Braams, 2000; Tourney and Ngwenya, 2014; Hauer et al., 2015). The inhibitory effect of EPS is thought to be caused by the formation of a protective layer on the mineral surface, slowing down mineral dissolution by decreasing its reactive surface area (Chen et al., 2000).

Both melanin and EPS furthermore play a role in substrate adhesion (Wessels, 1996; Nakari-Setala et al., 2002; Linder et al., 2005; Pihet et al., 2009). By attaching itself to a mineral surface, the cell gains several advantages (Dunne, 2002). Attachment allows cells to take up essential nutrients directly from the mineral, leading to a higher colonisation of minerals containing essential nutrients (Roberts, 2004; Rogers and Bennett, 2004). Surface attachment widens the scope of weathering mechanisms fungi have at their disposal. Unattached organisms can only use biochemical mechanisms, while attached organisms can also apply biomechanical mechanisms. Furthermore, fungal attachment influences the impact of the biochemical mechanisms; attachment has for example been shown to increase fungal siderophore excretion (Ahmed and Holmstrom, 2015).

The mineral used in this study to investigate these fungal weathering mechanisms is the nesosilicate olivine ($Fe_{0.2}Mg_{1.8}SiO_4$). Due to the availability of pure samples and its relatively simple dissolution mechanism, olivine's dissolution has been studied in varying environmental settings (Oelkers et al., 2018). This allows a better analysis of the effect of different conditions on the dissolution of olivine. Its presence on Mars (Olsen et al., 2015) and its potential role in carbon capture and storage (Schuiling and Krijgsman, 2006; Kohler et al., 2010) have further increased its significance. At pH < 9, olivine's abiotic dissolution is initially incongruent (i.e. Mg is preferentially released into the solution compared to Si) to become congruent after some hours (Luce et al., 1972; Pokrovsky and Schott, 2000; Rosso and Rimstidt, 2000; Oelkers, 2001; Martinez et al., 2014). The abiotic dissolution rate of olivine is dependent on the pH according to $r = ka_{H^+}^n$, with a reaction order (n) of 0.5 (Crundwell, 2014). Abiotically, etch pits are observed on acid-reacted and not on alkaline-reacted grains (Pokrovsky and Schott, 2000). The interdependence of microbial growth and the dissolution rate has been investigated by several studies (Bundeleva et al., 2014; Cai et al., 2013; Garcia et al., 2013; Oelkers et al., 2015; Seiffert et al., 2014; Shirokova et al., 2012). Two studies investigated the interactions between fungi and olivine, both observing an enhancement of olivine dissolution by fungal growth (Cai et al., 2013; Seiffert et al., 2014). These studies used the filamentous *Aspergillus niger* (Cai et al., 2013) and the non-filamentous *Knufia petricola* (Seiffert et al., 2014), two melanin-producing fungi.

The goal of this study is to investigate the effect of *Knufia petricola* A95 and its melanin-deficient mutant, *K. petricola* A95 Δ*Kppks*, on the dissolution kinetics of olivine at 25 °C and pH ~ 6. *K. petricola* A95 is a rock-inhabiting fungus belonging to the order of the Chaetothyriales. These rock-inhabiting fungi can be found in nearly every air-exposed rock ecosystem on Earth. Although *K. petricola* A95 does not produce hyphae, its production of melanin, EPS and siderophores (Gorbushina et al., 2008;

Favero-Longo et al., 2011; Breitenbach, 2018; Breitenbach et al., 2018) makes it usable as a model for bio-weathering studies. The melanin-deficient mutant Δ*Kppks* was created by knocking out *Kppks*, a gene which encodes a polyketide synthase type I (Knabe et al., 2017). Knocking out this gene caused at least a termination of melanin production, an increase of EPS production and a change in the EPS composition (Breitenbach, 2018). Therefore, the influence of these two fungal compounds – melanin and EPS – on olivine dissolution can be investigated. However, deletion of *Kppks* might have caused other phenotypic changes; this will be discussed further.

In this study we inoculated the olivine powder with both the wild type (WT) and the Δ*Kppks* mutant in batch and mixed flow reactors. Experimental dissolution experiments were well-controlled, and their geochemical, mineralogical and biological products were thoroughly analysed. Element concentration analysis by inductively coupled plasma optical emission spectroscopy (ICP-OES) of a time-series of medium solution samples provided olivine dissolution rates. Scanning electron microscope (SEM) imaging showed us the growth behaviour of specific cultures. And X-ray photoelectron spectroscopy (XPS) was used to investigate olivine's surface chemistry at a higher spatial resolution.

2. MATERIAL AND METHODS

2.1. Mineral and reacting media

The mineral used in the batch and mixed flow dissolution experiments was natural forsteritic olivine (Fo90) from San Carlos, Arizona (WARDs Chemicals, USA). The crystals were grounded with an agate mortar and pestle and the 63–125 μm size fraction was separated by dry sieving. The resulting powder was ultrasonically cleaned using acetone and deionised water (MilliQ, Millipore) (both 3 times) and dried at 65 °C until a stable weight was reached. The specific surface area (SSA) of the cleaned, unreacted (fresh) olivine powder was measured by the BET method (ASAP2020, Micromeritics, USA) at the Bundesanstalt für Materialforschung und -prüfung (BAM) according to International Organization for Standardization (2014) using krypton as an adsorptive gas. Since abiotically reacted samples gave a similar (within error) SSA as the unreacted fresh olivine, and since the SSA of biotically reacted samples could not be measured (due to the presence of cells on the mineral surface), only the SSA of the initial fresh olivine was used to calculate the olivine dissolution rates (Table 1). The reported uncertainties represent 2σ uncertainty and are based on the repeated analysis of the same sample. Electron microprobe analysis (JXA 8200, JEOL, USA) of the olivine, performed at Freie Universität Berlin according to Reed (2005), shows that this San Carlos olivine had a chemical composition of $Mg_{1.86}Fe_{0.19}SiO_4$.

The aqueous medium used in the dissolution experiment was a minimal nutrient solution containing all essential elements except the metal(loid)s, which should be obtained by dissolving olivine. Specifically, the nutrient medium solution (hereafter called CNPS medium) contained 298.9 μM of Na_2SO_4, 173.0 μM of K_2HPO_4*$3H_2O$, 9.95 μM of thiamine hydrochloride, 9.96 mM glucose*H_2O and 18.50 mM of NH_4NO_3. For the pH-buffered experiments, 11.11 mM of the pH buffer 2-(N-morpholino) ethanesulfonic acid hydrate (MES), set at pH 6, was added. The medium was autoclaved (Systec VX-75, 20 min at 120 °C and 100 kPa above atmospheric pressure) without glucose*H_2O and MES buffer as both were added afterwards using filter-sterilised stock solutions. For the batch experiments, an extra 4.98 mM glucose*H_2O was added at day 65 to prolong the experiment. For the abiotic mixed flow experiment at pH 3.5 ($MF_{ab,\ pH\ 3.5}$), MES was added, the pH was set at ca. 3.5 and the medium was autoclaved.

2.2. Fungal culturing and quantification

The fungal species used in this study, *Knufia petricola* A95, was isolated from a marble stone surface near the Philopappos monument in Athens, Greece by Gorbushina et al. (2008). The wild type and melanin-deficient mutant (*K. petricola* Δ*Kppks*) cultures were grown in malt extract broth (2.0 % malt extract, 0.1 % peptone from casein and 2.0 % glucose*H_2O) and incubated on a rotary shaker (100 rpm) at 25 °C in darkness. Before their weekly re-inoculation in fresh medium, cultures had to be disaggregated. This involved shaking the culture in a stainless-steel beaker together with 8 stainless-steel beads for 10 min at 30 Hz in a MM400 Mixer Mill (Retsch Laborgeräte, Haan, Germany) (Nai et al., 2013). New cultures were then setup by adding a hundredth volume of the disaggregated, one-week old culture to fresh medium. For inoculation of all conducted experiments, cells in their stationary growth phase were disaggregated and washed: once with 5 mM EDTA and once with the CNPS medium. To ensure the same amount of starter culture was used for each replicate (5×10^7 CFU l^{-1}), the cell number was quantified fast using a hemocytometer (Hecht-Assistent, Sondheim/Rhön, Germany), taking the average cell number from three grids.

The initial biomass was quantified as well by measuring the dry weight of the starter culture. The final biomass was estimated by subtracting the dry weight of the abiotic runs (consisting of olivine) from the dry weight of the abiotic runs (consisting of olivine and biomass). Uncertainties (Table 1) represent 1σ uncertainty and are based on the standard deviation of the technical replicates or the analytical uncertainty (i.e. 14%), whichever was highest. The mass of dissolved olivine was not significant compared to the final biomass.

2.3. Experimental set-up and procedure

The set-up and procedure of the growth, acidification, metal binding and dissolution experiments are described here. For a more detailed description of these experiments see Supplementary data 1.

2.3.1. Growth experiments

To characterise the growth of the wild type (WT) *K. petricola* and its melanin-deficient mutant (Δ*Kppks*), both were grown in batch reactors (Corning) at 25 °C for ca. 35 days. Six biological replicates of both WT and mutant were

Table 1
Comparison between fungal-induced and abiotic olivine dissolution in batch (B) and mixed flow (MF) experiments. Experiments at pH 6 were either abiotic (ab), in the presence of the wild type of *Knufia petricola* (WT) or in the presence of the Δ*Kppks* mutant of *K. petricola* (Δ*Kppks*). One additional abiotic experiment was run at pH 3.5 (ab, pH 3.5). All experiments were conducted at 25 °C, reactors were shaken at 150 rpm and incubated under continuous light (70 µmol photons $m^{-2}s^{-1}$). Biological replicates are numbered and consist of several technical replicates of which the means and uncertainties are shown. The nutrient solution for all these experiments was CNPS buffered with MES. Uncertainties (given in parenthesis) of biomass values represent 1σ and are based on the analytical uncertainty or the standard deviation of the technical replicates (whichever was highest). Uncertainties of SSA represent 2σ and are based on the repeated analysis of the same sample. Uncertainties of pH and grade of attachment values represent 2σ and are based on the analytical uncertainty or the standard deviation of the technical replicates (whichever was highest Uncertainties of the dissolution rates represent 2σ and are based on the propagated analytical uncertainties associated with the parameters in Equation 1 or 2, or on the standard deviation of the technical replicates (whichever was higher). The shown specific surface area (SSA) is of the unreacted olivine, while the shown pH values are of the fresh unreacted medium and the final reacted medium.

Experiment	Number of technical replicates	Duration (days)	SSA[a] (m^2 g^{-1})	Biomass (g ml^{-1}) × 10^{-3}		pH		Flow rate (ml min^{-1})	Dissolution rate (mol s^{-1} cm^{-2}) × 10^{-16}	Grade of attachment (%)
			Unreacted	Initial	Final	Fresh, unreacted medium	Final, reacted medium	Final	Final	Final
B_{ab}[b]	3	94	0.147 (±0.026)	n.a.[f]	n.a.	6.21 (±0.02)	6.20 (±0.21)		1.43 (±0.38)	n.a.
B_{WT}[c]	3	94	0.147 (±0.026)	n.a.	0.92 (±0.13)	6.21 (±0.02)	6.08 (±0.02)		10.4 (±2.4)	27 (±10)
$B_{\Delta Kppks}$[d]	2	94	0.147 (±0.026)	n.a.	0.501 (±0.070)	6.21 (±0.02)	5.92 (±0.06)		2.70 (±0.51)	4 (±4)
MF_{ab1}	1	37	0.142 (±0.026)	n.a.	n.a.	5.82 (±0.02)	6.02 (±0.02)	0.0349 (±0.0019)	3.37 (±0.76)	n.a.
MF_{ab2}	1	36	0.142 (±0.026)	n.a.	n.a.	5.81 (±0.02)	5,85 (±0.02)	0.0378 (±0.0023)	3.15 (±0.60)	n.a.
MF_{ab3}	1	42	0.110 (±0.020)	n.a.	n.a.	5.90 (±0.02)	5.90 (±0.02)	0.0305 (±0.0028)	3.93 (±0.79)	n.a.
MF_{WT1}	3	37	0.142 (±0.026)	n.a.	1.39 (±0.19)	5.82 (±0.02)	5.92 (±0.02)	0.0338 (±0.0052)	118 (±29)	27 (±12)
MF_{WT2}	3	36	0.142 (±0.026)	0.0129 (±0.0011)	0.81 (±0.26)	5.93 (±0.02)	5.81 (±0.02)	0.0320 (±0.0033)	20.4 (±4.2)	6 (±2)
MF_{WT3}	1	42	0.110 (±0.020)	0.00616 (±0.00022)	0.320 (±0.045)	5.90(±0.02)	5.87 (±0.02)	0.0295 (±0.0028)	16.8 (±3.4)	5 (±6)
$MF_{\Delta Kppks1}$	3	37	0.142 (±0.026)	n.a.	0.82 (±0.20)	5.82 (±0.02)	5.88 (±0.06)	0.0313 (±0.0058)	24 (±12)	4 (±4)
$MF_{\Delta Kppks2}$	3	36	0.142 (±0.026)	0.0304 (±0.0037)	1.72 (±0.24)	5.81 (±0.02)	5.72 (±0.04)	0.0337 (±0.0059)	20.1 (±7.2)	5 (±8)
$MF_{\Delta Kppks3}$	3	42	0.110 (±0.020)	0.01789 (±0.00025)	1.44 (±0.20)	5.90 (±0.02)	5.80 (±0.06)	0.0323 (±0.0034)	10.9 (±4.9)	5 (±6)
$MF_{ab,pH\ 3.5}$[e]	1	35	0.110 (±0.020)	n.a.	n.a.	2.79 (±0.02)	3.49 (±0.02)	0.0335 (±0.0066)	750 (±200)	n.a.

[a] SSA – the specific surface area, measured for the fresh unreacted olivine
[b] ab – abiotic control, a run without fungal inoculant
[c] WT – a run of *K. petricola* A95 wild type
[d] Δ*Kppks* – a run of *K. petricola* A95 Δ*Kppks*
[e] ab, pH 3.5 – abiotic control at pH 3.5
[f] n.a. – not analysed.

grown in liquid CNPS medium, buffered at pH 6, with 25 mg l^{-1} olivine (<63 μm). At selected times, the dry weight of the biomass was obtained by harvesting an entire reactor flask; the biomass was separated from the solution by centrifugation, dried at 65 °C and finally weighed. Note that the final amount of olivine (16 mg l^{-1}) in the abiotic reactor is insignificant compared to the final amount of biomass.

2.3.2. Acidification experiments

To determine the acidification capacity of the WT and mutant, both were grown in CNPS medium (pH 6.45) without a pH buffer but with 0.25 mg l^{-1} olivine. The experiment was run for 26 days as a technical triplicate. The pH was measured on solution samples taken over time.

2.3.3. Metal binding experiments

To determine the metal binding capacity of both *K. petricola* WT and Δ*Kppks*, it was impossible to use the cells from the dissolution experiments as the cells could not be separated from the olivine. Therefore, this experiment was run in the absence of olivine. This required the use of a medium with several micronutrients to allow growth and Mg, Si and Fe at a concentration similar to those in the dissolution experiments. To this end, *K. petricola* WT and Δ*Kppks* were grown in BG11 medium (Rippka et al., 1979) which was buffered at pH 6 using MES and supplemented with 10.1 mM glucose*H_2O, 407 μM $MgSO_4$*$7H_2O$, 250 μM SiO_2 and 23 μM NH_4Fe citrate. After 36 days of growth, the metal content of the biomass was measured by separating the biomass from the medium by centrifugation, weighing the dry biomass and dissolving it in concentrated acid as described in Supplementary data 1. Upon dissolution, the HNO_3 solution containing the dissolved biomass residue was analysed by ICP-OES. The aqueous Mg, Si and Fe concentrations at the beginning and end of the experiment was measured as well as a control. This experiment provided the percentages of the total Mg, Si and Fe in the reactors that was ultimately sequestered by the cells and thus the metal binding capacity of both strains.

2.3.4. Dissolution experiments

Dissolution experiments were carried out in batch and mixed flow reactor set-ups to quantify the abiotic dissolution of olivine and the effect of both the wild type fungus and its melanin-deficient mutant on olivine dissolution. The conditions and main results of all batch (B) and mixed flow (MF) experiments are shown in Table 1. Mixed flow experiments were repeated using different fungal starter cultures to take biological deviations into account. Results of each of these so-called biological replicates are given in Table 1. These results comprise the means and uncertainties of multiple technical replicates, i.e. runs of the same experiment at the same timepoint and using the same starter culture. An additional mixed flow abiotic control run was setup to determine the effect of an acidic pH on olivine dissolution ($MF_{ab,\ pH\ 3.5}$). Three additional abiotic batch experiments were run with either MilliQ water ($B_{ab,\ MQ}$), unbuffered CNPS medium ($B_{ab,\ unbuffered}$) or MES-buffered CNPS medium ($B_{ab,\ buffered}$) to determine the effect of the nutrient solution components on olivine dissolution. The results of these experiments are shown in Table D.1 of Supplementary data 1.

The batch dissolution experiments were performed with 4 (±0.001) g of ultrasonic cleaned olivine and 400 (±0.5) ml of the sterile CNPS nutrient solution, while the mixed flow dissolution experiments were performed with 1 (±0.001) g of ultrasonic cleaned olivine and 100 (±0.5) ml of the sterile CNPS nutrient solution. As the air phase of the reactors was in contact with the atmosphere through caps with built-in air filters (batch) and sterile air filters (mixed flow), oxygenated conditions are assumed in both. The reactor flasks were incubated in a climatic chamber (LT-36VL, Percival) under constant temperature (25.0 ± 0.1 °C), constant light source (70 μmol photons $m^{-2}s^{-1}$) and were shaken at 150 rpm. Note that the olivine and biomass in the reactors were not in suspension because excessive shaking is not suitable for biological growth. The flow rate for the mixed flow reactors was set at ca. 0.035 ml/min (see Table E.1, Supplementary data 2), giving a turnover time of ca. 2 days for the nutrient solution. Experiments were run until the biotic dissolution rates reached a constant value (i.e. ca. three months for the batch and over one month for mixed flow reactors).

Medium samples taken from the reactors were filtered (0.22 μm); 1 ml was used for pH measurement and 4 ml was acidified with HNO_3 (Merck, suprapur® grade) to a pH < 2 and stored in acid-cleaned, polypropylene falcon tubes at 4 °C prior to dissolved element analysis by ICP-OES. At the end of batch and mixed flow experimental runs, the dried biomass was weighed and samples were taken for SEM and XPS analyses.

2.4. Solution analysis and calculation of dissolution rates

Concentrations of dissolved Mg, Si and Fe were determined by inductively coupled plasma optical emission spectroscopy (ICP-OES, Varian 720-ES) analysis of the filtered and acidified solution samples in the "HELGES" laboratory at the German Research Centre for Geosciences (GFZ) Potsdam, Germany (von Blanckenburg et al., 2016). For a detailed description of this method see Schuessler et al. (2016). Details on sample preparation and the analytical protocol used in this study are given in Supplementary data 1. Note that the concentration values of the unreacted medium (medium blank, Fig. B.3, Supplementary data 1) and those of the medium flushed through the mixed flow set-up (procedure blank, Fig. B.3, Supplementary data 1) were subtracted from the concentration values from the batch and mixed flow samples, respectively. The detection limit for Mg was 0.010 ± 0.020 ppm, for Si it was 0.043 ± 0.022 ppm, and for Fe it was 0.004 ± 0.003 ppm. The analytical uncertainty used to interpret the sample results is conservatively estimated based on the accuracy and the precision of the repeated measurement of quality control standards (QC, typically close to 5% relative), or on twice the standard deviation of sample analysis of the technical experiment replicates, whichever was higher. Analytical results of QC standards for Mg, Fe and Si are given in Table B.1, Supplementary data 1. For

the Mg/Si and Fe/Si ratios, error bars in Fig. 3 represent 2σ uncertainty and are based on the combined propagated uncertainties of Mg and Si, and Fe and Si values, respectively. These (as mentioned) are based themselves on either the analytical uncertainty or on the standard deviation of the technical replicates, whichever was higher.

The pH of the filtered samples was measured at 25 °C with an analytical uncertainty of 0.01 pH unit, using a pH electrode (Blueline 25, Schott instruments) calibrated at pH 4, 7 and 10. Uncertainties in Table 1 and error bars in Fig. 1 represent 2σ uncertainty and are based on the analytical uncertainty or (if higher) on the standard deviation of the technical experiment replicates.

The olivine dissolution rate (r, mol cm^{-2} s^{-1}) for the batch experiments was calculated according to Daval et al. (2011):

$$r(t) = \frac{\Delta(C_{Mg})}{\Delta t \times m_{olivine}(t) \times SSA \times \eta_{Mg}} \quad (1)$$

where r(t) stands for the dissolution rate (mol cm^{-2} s^{-1}) based on the amount of Mg in solution at time t. $\Delta(C_{Mg})$ is the difference in molar amount of Mg between time t and t-Δt (i.e. two consecutive sampling points). Δt stands for the time (s) between different sampling points and $m_{olivine}(t)$ is the mass (g) of olivine in the bottle just before sampling at time t. The reactors were strongly shaken during sampling which resulted in a decrease of the mass of olivine at each sampling event by 0.054 (±0.010) g (based on repetitive sampling, n = 10). This gives an analytical uncertainty for the $m_{olivine}$ (t) of 1.9% (2σ). SSA stands for the specific surface area of olivine at the beginning of the experiment (in cm^2/g as measured by BET) and η_{Mg} for the stoichiometric coefficient of Mg in olivine (1.86 as measured by electron microprobe analysis).

For the mixed flow experiments the olivine dissolution rate was calculated according to:

$$r(t) = \frac{C_{Mg}(t) \times q(t)}{m_{olivine} \times \eta_{Mg} \times SSA} \quad (2)$$

where C_{Mg} stands for the outlet Mg aqueous concentration and q is the flow rate (l s^{-1}), both at time t. For the mixed flow experiment, the mass of olivine ($m_{olivine}$) is presumed constant (at 1 gram) since only medium solution flows out the reactors and only 0.2 % of the total mass of olivine is estimated to dissolve during the runs.

Uncertainties reported with the dissolution rates in Table 1 and the error bars in Fig. 4 represent 2σ uncertainty and are based on the combined analytical uncertainty calculated from the uncertainties of ICP-OES analysis, $m_{olivine}$ (t) (for batch), flow rate calculation (for mixed flow) and SSA analysis (i.e. propagated through equation 1 or 2), or on the standard deviation of the technical replicates, whichever was higher. The uncertainties of the mass of olivine ($m_{olivine}$) and the stoichiometric coefficient of Mg (η_{Mg}) are estimated at around 1% and are therefore deemed non-significant compared to the uncertainties on the other analysis.

2.5. Solid analysis

2.5.1. Surface analysis with XPS

The chemical composition of the near surface region of olivine and other Fe-containing minerals (as a reference) was determined by X-ray photoelectron spectroscopy (XPS). The XPS spectrum only probes the shallowest surface layers of the mineral: 63% of the signal originates from less than 26 Å, and 95% from less than 78 Å (Hochella and Carim, 1988). A detailed description of the used method is given in Supplementary data 1, Section C. Olivine harvested at the end of the dissolution experiments and unreacted olivine, goethite (Fe(III) oxyhydroxide), epidote (Fe(III) silicate), hornblende (Fe(II,III) silicate) and fayalite (Fe(II) silicate) were analysed to characterise the chemical state

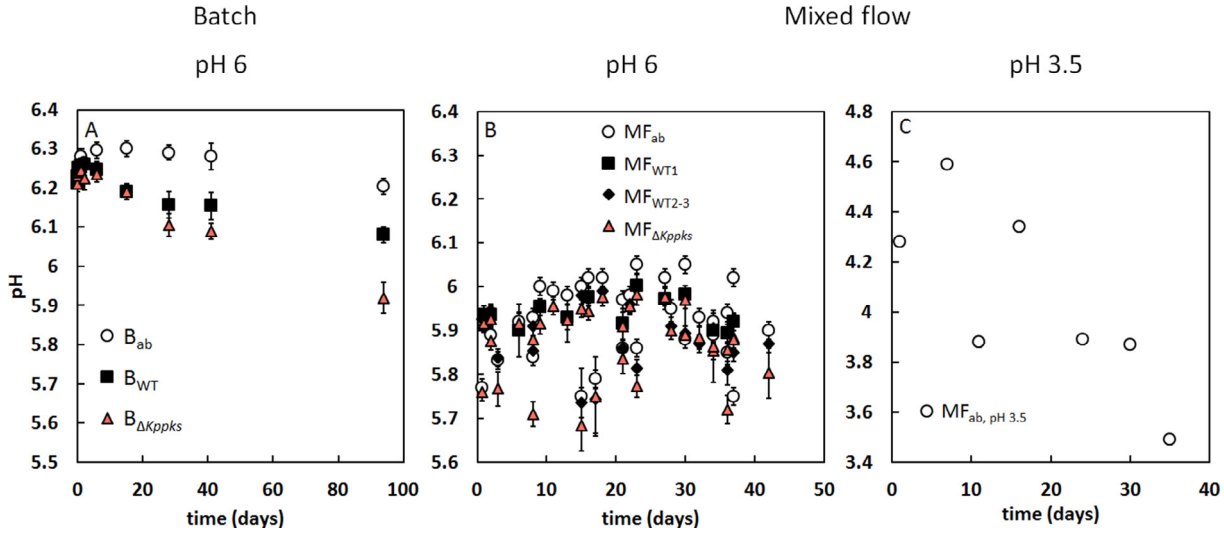

Fig. 1. Temporal evolution of the pH for batch (A) and mixed flow experiments at pH 6 (B) and pH 3.5 (C) with either wild type (WT), melanin-deficient mutant (Δ*Kppks*) or abiotic conditions (ab). Error bars represent 2σ uncertainty and are based on the analytical uncertainty or the standard deviation of the technical replicates, whichever is higher (if not visible they are smaller than the symbol).

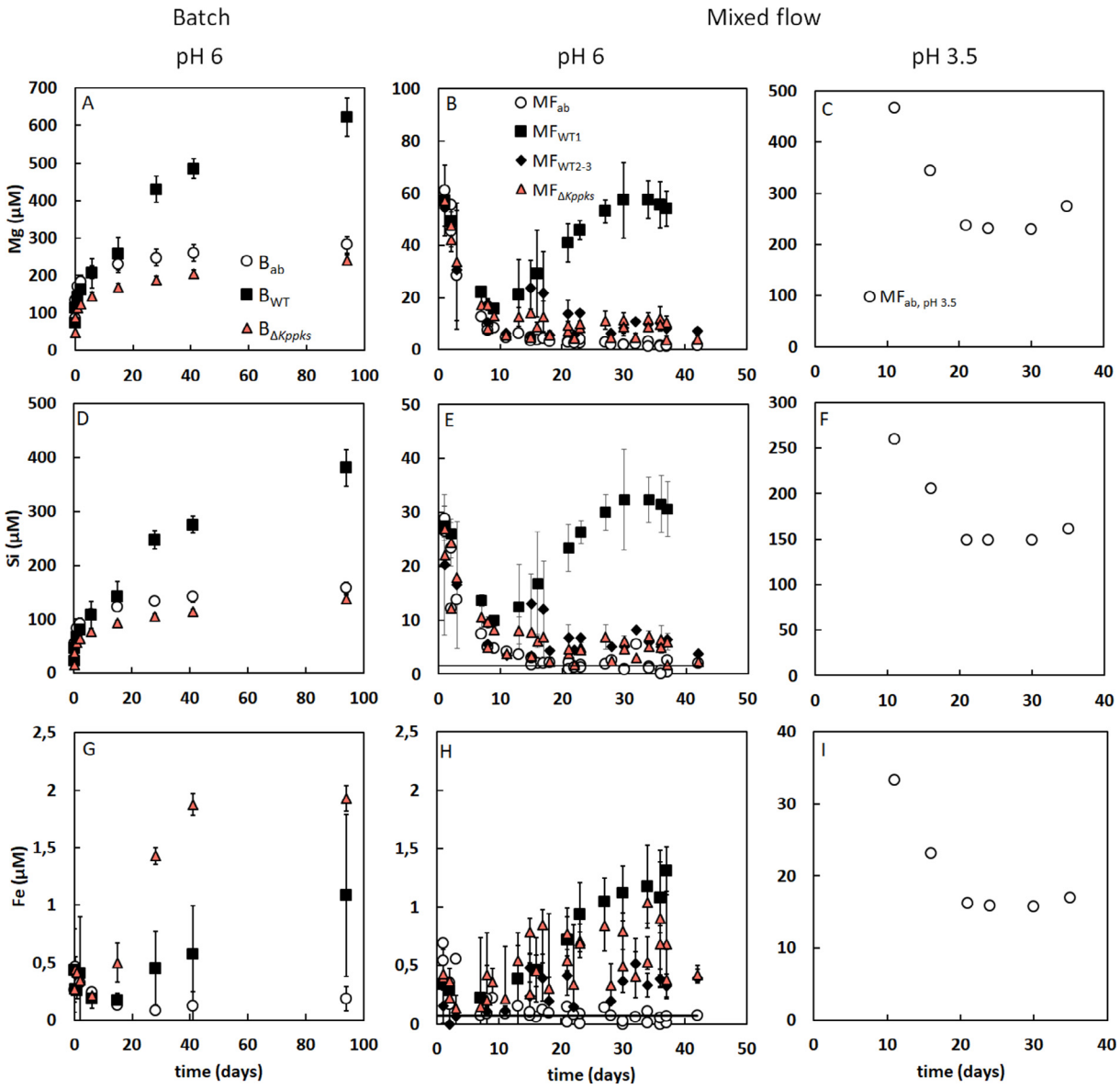

Fig. 2. Temporal evolution of the aqueous Mg concentration (µM) (A, B, C), Si concentration (µM) (D, E, F), and Fe concentration (µM) (G, H, I) for batch and mixed flow experiments at pH 6 and pH 3.5. Error bars represent 2σ uncertainty and are based on the analytical uncertainty or the standard deviation of the technical replicates, whichever is higher (if not visible they are smaller than the symbol). The Si and Fe concentrations for the abiotic mixed flow at pH 6 had values within the uncertainty of the procedure blank and below the ICP-OES detection limit, respectively (indicated by the lines in E and H) and are therefore not discussed.

of Fe at the surface of reacted olivine. Before analysis, some samples were ultrasonically cleaned with acetone to remove remaining attached cells (not all cells could however be removed). Neither ultrasonic cleaning nor autoclaving did have an observable effect on the XPS analysis (Table D.2, Supplementary data 1, unreacted samples).

Note that a high uncertainty of the transmission function in the energy region of the Mg peaks and the morphology of the powder samples hinder a quantitative analysis of the data. Therefore, the Mg results can only be used relatively. However, in the present study we were interested in the relative abundance of elements at the olivine surface and their modification upon olivine dissolution. Therefore, all elemental abundances were normalized to Si and expressed as X_{Me2p}/X_{Si2p}. Besides peak intensity, binding energies vary slightly when the state and the environment of an atom is changed (Carlson, 1975). Thus, we searched for shifts in the position of photoelectron peaks, especially in the case of Fe, in order to discern a change in the oxidation state or the appearance of a new phase. The uncertainty (2σ) of the binding energy is 0.4 eV, while the relative uncertainty of the atomic percentages was 20% (conservative estimate).

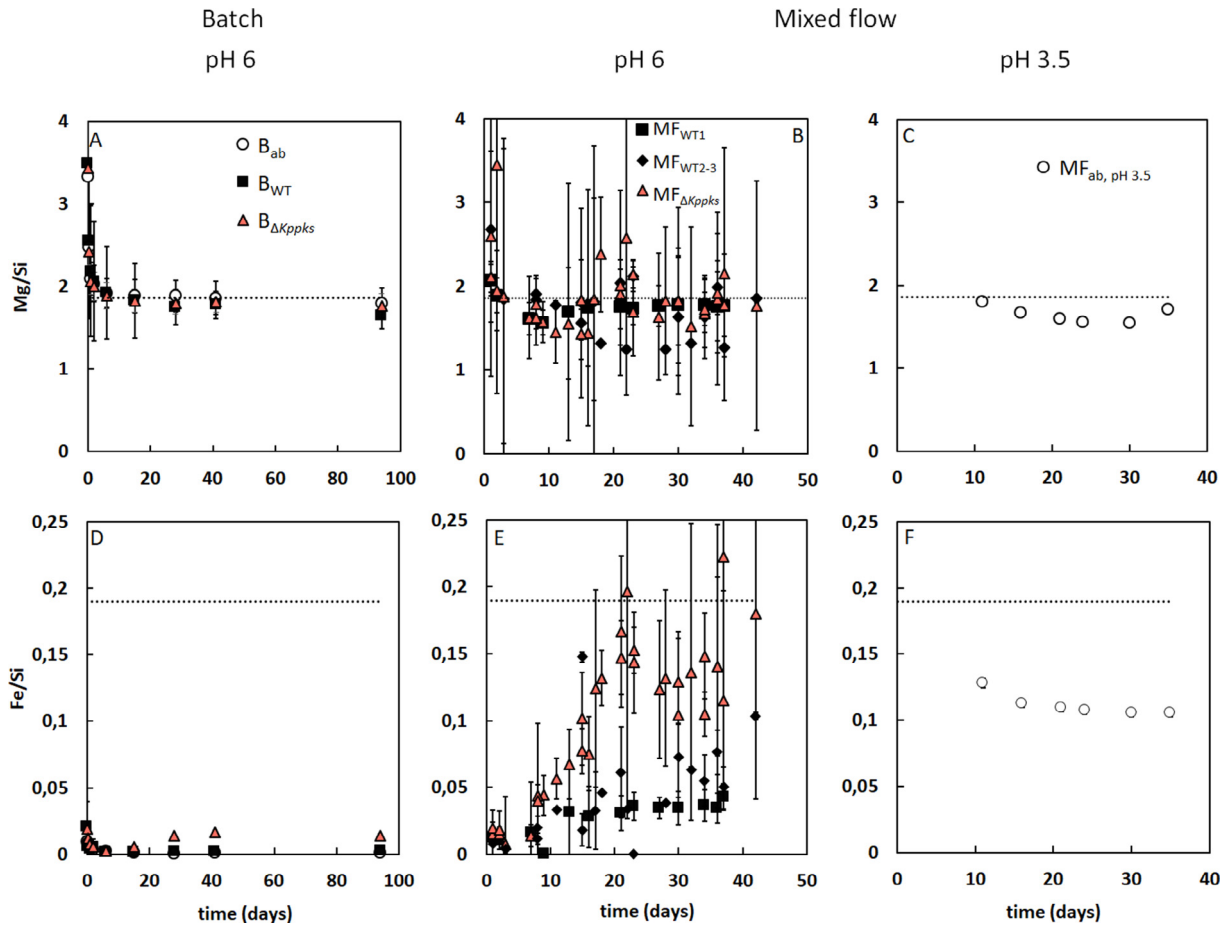

Fig. 3. Temporal evolution of the aqueous Mg/Si (A, B, C) and Fe/Si (D, E, F) ratios for batch and mixed flow experiments at pH 6 and pH 3.5. Stoichiometric dissolution is illustrated by the dotted line at Mg/Si = 1.86 in A, B and C and at Fe/Si = 0.19 in D, E and F. After a few days, all experiments had a stoichiometric Mg/Si release (A, B, C). Fe/Si release was however non-stoichiometric for all experiments except the mutant mixed flow runs at pH 6 (D, E, F). In general, the WT and the mutant generated almost stoichiometric Fe/Si ratios (D, E), indicating their ability to keep Fe in solution. The same is true for the abiotic experiment at pH 3.5 (F). The Mg/Si and Fe/Si values of the abiotic mixed flow experiments at pH 6 could not be calculated exactly and are therefore not given (B, E). The error bars represent 2σ uncertainty and are based on the combined propagated uncertainties of either Mg and Si (for Mg/Si) or Fe and Si (for Fe/Si) (if not visible they are smaller than the symbol).

2.5.2. Dissecting microscope analysis

The *grade of attachment* represents the percentage of olivine grains covered by a fungal biofilm (i.e. colonised grains). It was estimated by counting the colonised olivine grains using a dissecting microscope (Stemi 2000C, Zeiss) and dividing this number by the total number of olivine grains. The uncertainties reported in Fig. 4 represent 2σ and are based on the standard deviation of the technical replicates.

2.5.3. Scanning electron microscope analysis

The sample preparation used in this study for SEM analysis follows Spurr (1969). The fresh, unreacted olivine and solid samples taken at the end of each experiment were subsequently fixed with glutaraldehyde and osmium tetroxide and washed with phosphate-buffered saline (PBS). PBS was exchanged for ethanol by washing the samples with solutions with a gradual increasing ethanol concentration. The batch samples were subsequently air-dried. The samples from mixed flow runs were dried by critical point drying (Leica EM CPD300). Samples were then fixed onto adhesive carbon tape on a SEM sample-holder. After gold sputtering (10–15 nm), they were analysed by SEM (FEI XL30 with wolfram cathode, Thermo Fisher Scientific) at the BAM, Berlin to observe the growth behaviour of the wild type and mutant.

2.5.4. Measurement of ferric hydroxide precipitates by ultrasonic cleaning

To verify the presence of precipitated ferric hydroxides on the olivine surface, these precipitates were removed by ultrasonic cleaning. 1.000 g of either unreacted or abiotically reacted olivine powder was ultrasonically cleaned 3 times 15 minutes with 10.0 ml of MilliQ water. The supernatant was subsequently filtered (0.22 μm), acidified (pH < 2) and analysed by ICP-OES to measure the aqueous

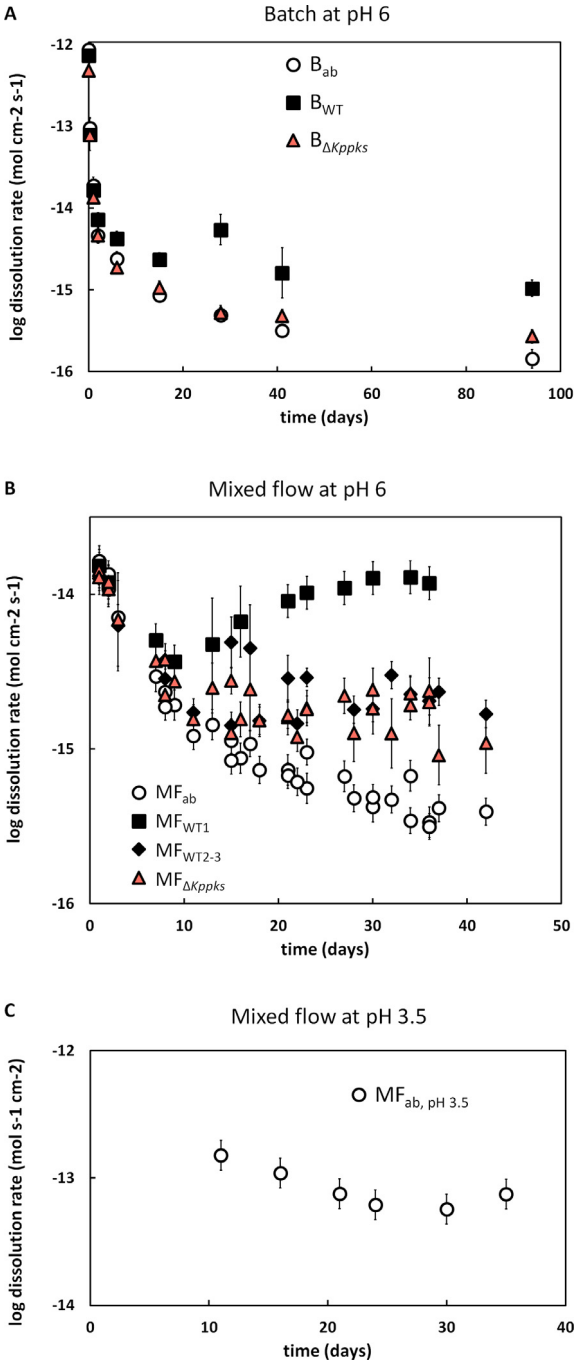

Fig. 4. The rates of abiotic and fungal-induced olivine dissolution based on the Mg concentrations measured in medium solution of batch (A) and mixed flow experiments at pH 6 (B) and pH 3.5 (C). Two WT runs in batch and mixed flow (i.e. B_{WT} and MF_{WT1}) yielded a significantly higher dissolution rate than the other biotic runs. Error bars represent 2σ uncertainty and are based on the propagated analytical uncertainties associated with the parameters in Eq. 2 or 3 or the standard deviation of the technical replicates whichever is higher (if not visible they are smaller than the symbol).

Fe concentration. Supernatant of unreacted and abiotically reacted olivine which was not ultrasonically treated was analysed as a control.

2.6. Statistical analysis

For the growth, the acidification and the metal binding experiments, the differences between the results of the WT and Δ*Kppks* were proven significant by an unpaired two-sample t test at $p < 0.05$. The differences between the dissolution rates of the abiotic runs, biotic unattached runs and biotic attached runs were analysed using one-way analysis of variance (ANOVA) together with Duncan's multiple range test at $p < 0.05$.

To analyse the dependence of the dissolution rates on the pH, biomass or grade of attachment, the rates of each technical replicate were plotted against the activity of protons to the power of 0.5 (i.e. $a_{H+}^{0.5}$, based on Pokrovsky and Schott (2000)), the biomass or the grade of attachment (%), respectively (Fig. 8). Therefore, for the dependence on the biomass or grade of attachment the number of data points (n) is 5 for the batch and 16 for the mixed flow experimental results; while for dependence on pH, n equals 8 and 19 for batch and mixed flow runs, respectively. From these plots the coefficient of determination – R squared (R^2) – was determined without taking the uncertainties into account.

3. RESULTS

3.1. Growth, acidification and metal binding experiments

The growth experiment, which comprised the inoculation of the WT and the Δ*Kppks* mutant in CNPS medium with 25 mg l^{-1} olivine, generated growth curves for both strains (Fig. D.1, Supplementary data 1). These indicate that the exponential growth phase lasted from day 4 to 20. Based on this exponential phase, the WT had a growth constant (μ) of 0.00170 ± 0.00019 h^{-1} while the mutant had one of 0.00205 ± 0.00015 h^{-1}. In general, the final biomass of Δ*Kppks* reached a significantly ($p < 0.05$) higher value: the mean of the six replicates was 470 ± 110 mg/l for Δ*Kppks* compared to 326 ± 92 mg/l for the WT. The variation at the beginning of the experiment is likely caused by the difficulty in estimating the starting biomass with the hemocytometer.

The acidification experiment, constituting the growth of the WT and mutant in unbuffered CNPS medium (pH 6.45) with 0.25 mg l^{-1} olivine for 26 days, showed that both strains decreased the pH of unbuffered medium to 3.12 ± 0.12 and 2.83 ± 0.06, respectively (significantly different, $p < 0.05$, Fig. D.2, Supplementary data 1).

Both the WT and mutant were as well able to bind Mg, Si and Fe from a buffered nutrient solution (BG11 medium amended with Mg, Si and Fe) without olivine in the metal binding experiment. The Mg, Si and Fe contents of WT and Δ*Kppks* cells harvested from this experiment are given in Table 2. The wild type cells were able to bind significantly more Mg and Fe than the mutant. Fe was taken up most of all: the WT and mutant had a Fe content of 3000 ± 1100 μg g^{-1} and 1720 ± 300 μg g^{-1}, respectively. However, both bound almost all Fe initially present in the medium: 98.5% and 95.7% for the WT and mutant, respectively (Table 2). The

Table 2
The capacity of the wild type and melanin-deficient mutant Δ*Kppks* to bind aqueous Mg, Si and Fe. The Mg, Si and Fe content of the fungal biomass (μg g^{-1}) and the percentages of Mg, Si and Fe bound in the biomass (%), derived from the metal binding experiment. Uncertainties represent 2σ and are based on the analytical uncertainty or (if higher) the standard deviation of the technical replicates.

	K. petricola WT	*K. petricola* Δ*Kppks*
Mg (μg g^{-1})	650 ± 160	470 ± 110
% Mg bound	2.5	2.8
Si (μg g^{-1})	320 ± 110	249 ± 30
% Si bound	1.9	2.4
Fe (μg g^{-1})	3000 ± 1100	1720 ± 300
% Fe bound	98.5	95.7

potential Fe binding capacity of both strains is therefore probably higher.

3.2. Dissolution experiments

3.2.1. Attachment capacity of fungal strains

The degree to which the different WT runs attached to the olivine varied. Estimation of the attachment by stereomicroscopy revealed that the cultures from batch WT run B_{WT} and mixed flow WT run MF_{WT1} had a so-called grade of attachment (for calculation see method section) of 27 ± 10 % and 27 ± 12 %, respectively (Table 1). This is significantly higher than the grades of attachment of the other WT runs (i.e. MF_{WT2} and MF_{WT3}) which were 5 ± 6 % and 6 ± 2 % (Table 1). The grade of attachment of the Δ*Kppks* batch and mixed flow runs was similar and ranged from 4 ± 4 % to 5 ± 8 % (Table 1). The differences in attachment to olivine were also apparent from visual inspection of the reactors. The fungal cultures of runs B_{WT} (Fig. D.3A, Supplementary data 1) and MF_{WT1} grew directly on the olivine as opposed to the other set-ups (Fig. D.3B, Supplementary data 1 for $B_{\Delta Kppks}$).

3.2.2. Evolution of biomass and pH with time

In batch experiments, the biomass concentrations of the wild type (B_{WT}) and the mutant ($B_{\Delta Kppks}$) reached final values of $9.2 \pm 1.3 \times 10^{-4}$ and $5.01 \pm 0.70 \times 10^{-4}$ g ml^{-1}, respectively. In the mixed flow runs the final biomasses were $1.39 \pm 0.19 \times 10^{-3}$ g ml^{-1} for the attached WT (MF_{WT1}), ranged from 0.32 10^{-3} to 0.81 10^{-3} g ml^{-1} for the unattached WT (MF_{WT2-3}) and 0.82×10^{-3} to 1.72×10^{-3} g ml^{-1} for Δ*Kppks* ($MF_{\Delta Kppks}$) (Table 1).

The temporal evolution of the pH of batch and mixed flow experiments is illustrated in Fig. 1. In the batch experiments, the pH of the biotic set-ups slightly decreased from 6.20 (±0.02) to 6.08 (±0.02) for the WT (B_{WT}) and 5.92 (±0.06) for the Δ*Kppks* ($B_{\Delta Kppks}$) (Fig. 1A), even though the medium was buffered at pH 6.2 using MES. For the abiotic set-up (B_{ab}), the pH stayed constant with a final value of 6.20 (±0.02). For the mixed flow experiments, the final pH values of all experimental runs (MF_{ab}, MF_{WT} and $MF_{\Delta Kppks}$) ranged from 5.70 (±0.02) to 6.02 (±0.02) (Fig. 1B), without clear differences between biotic and abiotic runs. The pH of the abiotic mixed flow experiment at pH 3.5 ($MF_{ab,\ pH\ 3.5}$) ranged from 4.59 (±0.02) to a final pH value of 3.49 (±0.02) (Fig. 1C).

3.2.3. Element release from olivine with time

3.2.3.1. Mg and Si. The release of Mg and Si in the abiotic batch experiment (B_{ab}) at pH 6 was non-stoichiometric during the first two days of the experiment, with a preferential release of Mg (Fig. 3A), and considerably slowed down over time (Fig. 2A and D). Final Mg and Si aqueous concentrations in the abiotic set-up were 282 ± 22 and 157 ± 10 μM, respectively.

In abiotic mixed flow reactors at pH 6 (MF_{ab}), the Mg and Si concentrations in solution also decreased considerably with time to final concentrations of ~ 1 μM for Mg and within the uncertainty of the procedure blank for Si (Fig. 2B and E). At pH 3.5 ($MF_{ab,pH\ 3.5}$), the concentrations of Mg and Si only slightly decreased to a final value of 275 μM for Mg and ~161 μM for Si (Fig. 2C and F). Due to the low final Si concentrations (being not significantly different from the procedure blank), Mg/Si ratios could not be calculated for abiotic runs at pH 6 and therefore aren't reported. For the experiment performed at pH 3.5, release of Mg was almost stoichiometric (Fig. 3C).

In biotic batch runs, the aqueous Mg and Si concentrations of the wild type (B_{WT}) started to deviate from the abiotic runs after 8 days and reached final Mg and Si concentrations of 622 ± 51 and 379 ± 34 μM, respectively. Mg and Si release in the mutant runs ($B_{\Delta Kppks}$) were close to those in the abiotic runs with final Mg and Si concentration of 241 ± 15 and 137 ± 7 μM, respectively. Just as in the abiotic batch run, olivine dissolution was initially non-stoichiometric with respect to Mg but turned stoichiometric after two days (Fig. 3A).

In biotic mixed flow reactors, the Mg and Si concentrations for mutant runs ($MF_{\Delta Kppks}$), and the unattached WT runs MF_{WT2-3} initially decreased but reached steady state values around 7 μM for Mg and 4 μM for Si (Fig. 2B and E). For the attached WT run MF_{WT1}, the Mg and Si concentrations increased again after reaching a minimum at day 8; the final Mg and Si concentrations were 53.9 ± 6.7 and 30.6 ± 5.1 μM, respectively. In these biotic runs, Mg was initially preferentially released over Si, but final Mg/Si ratios were not significantly different from that of olivine (Fig. 3B).

Applying the Mg and Si concentrations of both the WT and mutant from the metal binding experiment (Table 2) to the final respective WT and mutant biomass in the dissolution experiments shows that ca. 6% and 1% of the olivine-released Mg and Si, respectively, could have been sequestered by the cells of both strains.

3.2.3.2. Fe. The dissolved Fe concentration in the abiotic batch experiment (B_{ab}) reached a final value of 0.18 ± 0.10 μM (Fig. 2G). Release of Fe in these experiments was far from stoichiometric (Fig. 3D).

In the mixed flow reactors, the final Fe concentration was below the ICP-OES detection limit of 0.07 μM for the abiotic run at pH 6 (MF_{ab}, Fig. 2H), and reached 17.02 ± 0.31 μM for the run at pH 3.5 ($MF_{ab,\ pH\ 3.5}$, Fig. 2I). Due to the low final Si and Fe concentrations

(not significantly different from the procedure blank and below the ICP-OES detection limit, respectively), Fe/Si could not be calculated for abiotic runs at pH 6 and therefore isn't reported. Release of Fe from the dissolution experiment at pH 3.5 was slightly non-stoichiometric (Fig. 3F).

The aqueous Fe concentration in the batch reactors with the mutant ($B_{\Delta Kppks}$) increased to a final value of 1.92 $\pm$ 0.11 μM, significantly higher than for batch reactors with the wild type (1.07 $\pm$ 0.70 μM) (B_{WT}, Fig. 2G). Just as in the corresponding abiotic batch run, olivine dissolution was far from stoichiometric with respect to Fe in the biotic batch runs (Fig. 3D).

For the mixed flow runs, the aqueous Fe concentrations were 1.31 $\pm$ 0.20 μM for the attached WT (MF_{WT1}) and ranged from 0.4 to 0.7 μM for the mutant and unattached WT ($MF_{\Delta Kppks}$ and $MF_{WT2\text{-}3}$). The Fe/Si ratios in these biotic runs were still non-stoichiometric but became more stoichiometric over time, with the mutant runs ($MF_{\Delta Kppks}$) generating the most stoichiometric Fe/Si ratios (Fig. 3E).

Based on the Fe content of both the WT and mutant (metal binding experiment, Table 2), the final biomass of both strains could theoretically incorporate all olivine-released Fe (even in the case of stoichiometric dissolution).

The amount of precipitated Fe on the abiotically reacted olivine surface was estimated by removing these precipitates through ultrasonic treatment and subsequent analysis of the supernatant. Abiotically reacted olivine which was treated as such delivered 0.21 μmol of Fe per gram of olivine. This accounts for 12% of all Fe which was stoichiometrically released from olivine during dissolution. Without ultrasonication, unreacted and abiotically reacted olivine did not deliver aqueous Fe (i.e. below the limit of detection). Analyses of the supernatant of unreacted olivine which was ultrasonically treated did not reveal aqueous Fe either.

3.2.4. Olivine dissolution rate as a function of time

In abiotic batch experiments, the rates of olivine dissolution at pH 6 considerably decreased with time for abiotic runs (B_{ab}): the dissolution rate decreased by 4 orders of magnitude reaching a final value of 1.43 ($\pm$0.38) $\times$ 10^{-16} mol cm^{-2} s^{-1} (Table 1 and Fig. 4A). For the abiotic mixed flow runs (MF_{ab}) at pH 6, the olivine dissolution rates exhibited a similar decrease with time as for the batch, reaching values ranging from 3.15 $\times$ 10^{-16} to 3.93 $\times$ 10^{-16} mol $cm^{-2}s^{-1}$ after $\sim$ 40 days (Table 1 and Fig. 4B). At pH 3.5 ($MF_{ab,\ pH\ 3.5}$) however, the dissolution rate reached a much higher final value of 7.5 ($\pm$2.0) $\times$ 10^{-14} mol cm^{-2} s^{-1} (Table 1 and Fig. 4C).

The olivine dissolution rates of the wild type and mutant batch runs also decreased but to a smaller extent. The final rates of the WT (B_{WT}) were almost four times higher than those of the mutant ($B_{\Delta Kppks}$): 10.4 ($\pm$2.4) $\times$ 10^{-16} and 2.70 ($\pm$0.51) $\times$ 10^{-16} mol $cm^{-2}s^{-1}$, respectively (Table 1, Fig. 4A). For the mixed flow, the dissolution rates of the wild type (MF_{WT}) and mutant ($MF_{\Delta Kppks}$) both initially decreased and started to level off after 7 to 15 days of reaction (Fig. 4B). The dissolution rates of the attached WT (MF_{WT1}) even started to increase again at day 7 and rates remained stable at 118 ($\pm$29) $\times$ 10^{-16} mol $cm^{-2}s^{-1}$. The dissolution rates for the unattached WT ($MF_{WT2\text{-}3}$) were lower and ranged from 16.8 $\times$ 10^{-16} to 20.4 $\times$ 10^{-16} mol $cm^{-2}s^{-1}$,while for the mutant ($MF_{\Delta Kppks}$) they ranged from 10.9 $\times$ 10^{-16} to 24 $\times$ 10^{-16} mol $cm^{-2}s^{-1}$ (Table 1, Fig. 4B). In conclusion, all biotic dissolution rates were faster than the abiotic ones ($p < 0.05$) and the dissolution rates for the attached wild type (MF_{WT1}) (i.e. 118 $\times$ 10^{-16} mol $cm^{-2}s^{-1}$) was significantly ($p < 0.05$) higher – by almost one order of magnitude – than those of the unattached WT and mutant runs.

3.2.5. XPS analysis of the olivine surface chemistry

The olivine surface compositions (Mg/Si, Fe/Si, O/Si and C/Si) together with the binding energies for O1s, Fe2p and C1s from XPS analyses are given in Table 3 and Table D.2 of Supplementary data 1. All corresponding Fe2p, O1s and C1s spectra are shown in Supplementary data 2. The abiotically reacted surface from batch (B_{ab}) and mixed flow (MF_{ab}) experiments at pH 6 had a similar Mg/Si as the unreacted olivine (Table 3). The abiotic surface was however enriched in Fe (i.e. a higher Fe/Si ratio than the unreacted olivine) and contained more oxygen (an increased O/Si ratio). At pH 3.5, the surface did have a significantly ($p < 0.05$) lower Mg/Si ratio, indicating Mg depletion. The olivine surface which reacted at pH 3.5 was as well enriched in Fe and O. The presence of the $Fe2p_{3/2}$ and $Fe2p_{1/2}$ peaks around 709.5 eV and 723.0 eV, respectively, for the unreacted olivine agree with previously published XPS analysis of freshly ground olivine (Seyama and Soma, 1987) and indicate that Fe was present as Fe^{2+}. These $Fe2p_{3/2}$ and $Fe2p_{1/2}$ peaks are absent (or have a lower surface area) for the abiotically reacted olivine, indicating the oxidation of this ferrous Fe (Biesinger et al., 2011). The O1s peak of the abiotically reacted olivine shows a shoulder at 532.6 eV which was not observed for the unreacted surface and indicates the presence of organic C (Table 3). This organic C came likely from the environment during sample handling and/or from the nutrient solution and is shown as well by the high C/Si ratios (Table 3). The XPS spectra of abiotically reacted olivine were compared to those of unreacted olivine, goethite (Fe(III)OOH), epidote ($Fe(III)Si_2O_7$), hornblende ($Fe(II,III)Si_4O_{11}$) and fayalitic olivine ($Fe(II)SiO_4$) (Supplementary data 4 and 5). The position of the main Fe2p and O1s peaks and the presence of certain satellite Fe2p peaks of abiotically reacted olivine align best with those of epidote.

The chemical composition of the olivine surface which reacted with the attached WT, unattached WT or the mutant was similar for the batch and mixed flow (Table 3) but should be analysed with caution as the surface could not entirely be cleared of cells. The Mg/Si values of the biotically reacted olivine surface were not significantly different to those of the abiotically reacted surface. The Fe/Si values of the biotic samples were significantly higher than those of the unreacted olivine, while (occasionally) significantly smaller than those of the abiotic samples. The O/Si ratios for biotic samples were significantly higher than for the abiotic samples, either indicating the presence of remaining cells or the precipitation of ferric hydroxides.

Table 3
XPS analysis of selected samples of unreacted olivine and reacted olivine from the batch and mixed flow experiments. Before XPS analysis, samples were either ultrasonically cleaned (US) or not (~~US~~). The shown unreacted sample was autoclaved (AC). The shown Mg/Si, Fe/Si, O/Si and C/Si data are based on the atomic percentages and are accompanied by the propagated uncertainty based on the 95% confidence interval. The binding energies (eV) of the $Fe2p_{1/2}$, $Fe2p_{3/2}$, O1s and C1s peaks are given together with their uncertainty of 0.4 eV. The results of the XPS analyses of all samples are presented in Table D.2 of Supplementary data 1, while all Fe2p, O1s and C1s spectra are shown in Supplementary data 3. The Mg/Si values can only be compared between the different set-ups (i.e. relatively) since Mg could not be quantified exactly by XPS.

		Batch			Mixed flow			
	Unreacted US, AC	Abiotic US	WT US	Δ*Kppks* US	Abiotic US	WT2[a] US	Δ*Kppks* US	Abiotic, pH 3.5 ~~US~~
Mg/Si	1.57 (±0.44)	1.63 (±0.46)	1.56 (±0.44)	1.27 (±0.36)	1.46 (±0.41)	1.44 (±0.41)	1.49 (±0.42)	0.96 (±0.27)
Fe/Si	0.105 (±0.030)	0.50 (±0.14)	0.40 (±0.11)	0.215 (±0.061)	0.214 (±0.061)	0.253 (±0.071)	0.184 (±0.052)	0.40 (±0.11)
O/Si	4.4 (±1.2)	4.6 (±1.3)	9.1 (±2.6)	7.8 (±2.2)	5.4 (±1.5)	9.5 (±2.7)	8.4 (±2.4)	7.3 (±2.1)
C/Si	2.08 (±0.59)	1.15 (±0.32)	11.8 (±3.3)	10.1 (±2.8)	3.8 (±1.1)	12.6 (±3.6)	11.5 (±3.3)	5.8 (±1.6)
$Fe2p_{3/2}$	709.4	711.2	(709.3) [b]	(709.2)	(709.1)	(709.0)	(709.1)	(709.0)
(eV)	710.9		711.4	710.6	710.9	711.1	710.7	711.7
$Fe2p_{1/2}$	723.1	724.6	(722.5)	(722.4)	(722.8) 724.6	(723.0)	(722.9)	(722.1)
(eV)	724.6		724.1	724.2		724.7	724.5	725.1
O1s (eV)	531.2 (532.4)	531.3 (532.6)	531.1 532.7 (534.4)	530.9 532.6 (534.6)	530.9 (532.2)	531.0 532.5	531.0 532.6	531.1 (532.5)
C1s (eV)	285.0 (285.7) (286.8) (289.1)	285.0 (285.8) (286.9) (289.0)	284.9 286.4 (288.1) (289.8)	285.0 286.4 (288.0) (289.6)	284.9 286.4 (288.5)	285.0 286.4 (288.3)	285.0 286.4 (288.1)	285.0 286.4 (288.4)

[a] The number indicates the specific WT run, WT run 2 was unattached.
[b] Binding energies in parenthesis indicate a shoulder or peaks with a lower surface area.

The binding energies of the Fe2p peaks agree with those of the abiotically reacted surface: Fe was present as Fe^{3+}. The olivine surface reacted in the presence of both WT and mutant also showed an additional O1s peak around 532.5 eV, again indicating the presence of organic C. The presence of biomass was as well shown by the increase in C/Si ratios and more prominent C1s peaks around 286.5 eV (Table 3).

3.2.6. Microscopical observations of the biofilm by SEM

SEM images of olivine-fungus samples taken out of the reactors after the olivine dissolution experiments are shown in Figs. 5 and 6. The abiotic set-ups do not show microbial growth (Fig. 5A, D and H). The biotically reacted grains showed the growth behaviour of the fungal cultures (Fig. 5B, C, E, F and G): certain WT runs showed an enhanced ability to attach to the olivine grains, confirming the reported grades of attachment (Table 1).

In the abiotic experiments, the olivine grains at pH 6 did not show etch pits (Fig. 5AF and D), while at pH 3.5 they did (Fig. 5H). The extensive etching patterns on the surface of the olivine grains at pH 3.5 seem to be depended on the crystal orientation as etching was not observed on every surface.

Extracellular polymeric substances (EPS) were visible around most cells and were in general thicker around the mutant (Fig. 6B) than around the wild type cells (Fig. 6A). The thread-like appearance of the EPS is an artefact of the sample preparation (more specifically the ethanol dehydration) (Breitenbach, 2018). The mineral precipitates caught in the mutants' EPS could not be defined (Fig. 6B).

4. DISCUSSION

In our experiments, the rates of fungal-induced olivine dissolution were higher than those of abiotic olivine dissolution. To put these dissolution rates into context, we compared them with the equations reported by Rimstidt et al. (2012) which are based on literature data (Fig. 7). This revealed that the abiotic dissolution rates in batch and mixed flow runs at pH 6 were about 2.7 and 2.0 orders of magnitude lower, respectively, than literature data reported for the same pH (Fig. 7). In contrast, the abiotic dissolution rate measured in this study at pH 3.5 using a mixed flow reactor is in good agreement with literature data (log r of -13.1 mol cm^{-2} s^{-1} compared to -12.5 mol cm^{-2} s^{-1} of Rimstidt et al. (2012), Fig. 7). ICP-OES and XPS analyses showed that the surface of the abiotically reacted olivine was enriched in ferric Fe. We will demonstrate that this ferric Fe was involved in the inhibition of olivine dissolution.

The similarity between the olivine dissolution rate of WT run MF_{WT1} and the abiotic rates from the literature (log r of -13.9 mol cm^{-2} s^{-1} compared to -13.6 mol cm^{-2} s^{-1}, Fig. 7) suggests that attachment of the *K. petricola* to the olivine surface suppresses the dissolution inhibition. We will further discuss the mechanisms by which *K. petricola* could interact with Fe upon attachment to the olivine, thereby reducing the inhibiting effect of ferric Fe.

4.1. Abiotic olivine dissolution

The abiotic dissolution rates at pH 6 are lower than the rates derived from the modelling study of Rimstidt et al. (2012) (Fig. 7). In fact, they continuously decreased over time in both batch and mixed flow reactors (Fig. 4A and 4B) indicating the inhibition of olivine dissolution. An important observation is that as olivine dissolution rates decreased, olivine-released Fe kept being removed from solution, as evidenced by the very low Fe/Si values of the abiotic runs (Fig. 3D). XPS analyses of the abiotically reacted olivine surface show higher Fe/Si values for the reacted surface compared to the unreacted surface (Table 3), indicating that released Fe precipitated on the olivine surface. The shift of the Fe2p peaks to higher binding energies upon reaction indicates that the released ferrous Fe had oxidised and was present on the surface as ferric Fe. The similarities between the binding energies of the satellite Fe2p peaks and the main Fe2p and O1s peaks of the abiotically reacted olivine and those of the unreacted epidote (Supplementary data 4 and 5) suggest that the surface layer of the reacted olivine consists of a Fe(III)-containing silicate rather than a Fe(III) hydroxide. Since the adsorption of Fe(III) is unlikely at pH 6 (due to its low solubility), the observed Fe(III) silicate is probably formed by *in-situ* oxidation of ferrous Fe which was already present in the unreacted olivine. However, this would not explain the Fe (III) enrichment of the reacted olivine surface. We therefore cannot exclude the precipitation of a thin ferric hydroxide layer. The precipitation of Fe(III) hydroxides on olivine's surface is supported by the presence of Fe in the supernatant of ultrasonically cleaned, abiotically reacted olivine.

This Fe(III) enrichment of the surface layers (Table 3) together with the decreasing and overall low olivine dissolution rates at pH 6 (Fig. 7) and the absence of Fe in solution (Fig. 3D and E), all demonstrate that the Fe(III) enrichment of the olivine surface layers caused the strong inhibition of olivine dissolution. The inhibiting effect of ferric Fe at pH 6 is shown as well by the dissolution experiment at pH 3.5: at this pH the olivine dissolution rate agreed with the presented model of Rimstidt et al. (2012) (Fig. 7) while less Fe was removed from solution (Fig. 3F). The latter is in agreement with the slower oxidation rate of Fe(II) at lower pH (Millero, 1985; Singer and Stumm, 1970). Based on the aqueous Fe/Si ratio (Fig. 3F), the Fe-rich surface layer detected at pH 3.5 by XPS measurements (Table 3) is probably not thick enough to inhibit olivine dissolution.

The remaining question is why most olivine dissolution studies, and thus the model of Rimstidt et al. (2012), do not show an inhibition by Fe. These studies did not report the oxidation of Fe(II) as their experiments were performed either for shorter reaction times; at high flow rates, resulting in short residence time of the fluid in the reactor; with bubbling of N_2 in the fluid, removing most of dissolved oxygen; at acidic pH; or simply using Fe-free forsterite (Wogelius and Walther, 1991; Pokrovsky and Schott, 2000; Oelkers, 2001; Golubev et al., 2005; Hanchen et al., 2006; Maher et al., 2016). These settings prevent significant Fe oxidation over the course of the dissolution experiments. In contrast, the design of both batch (open to the

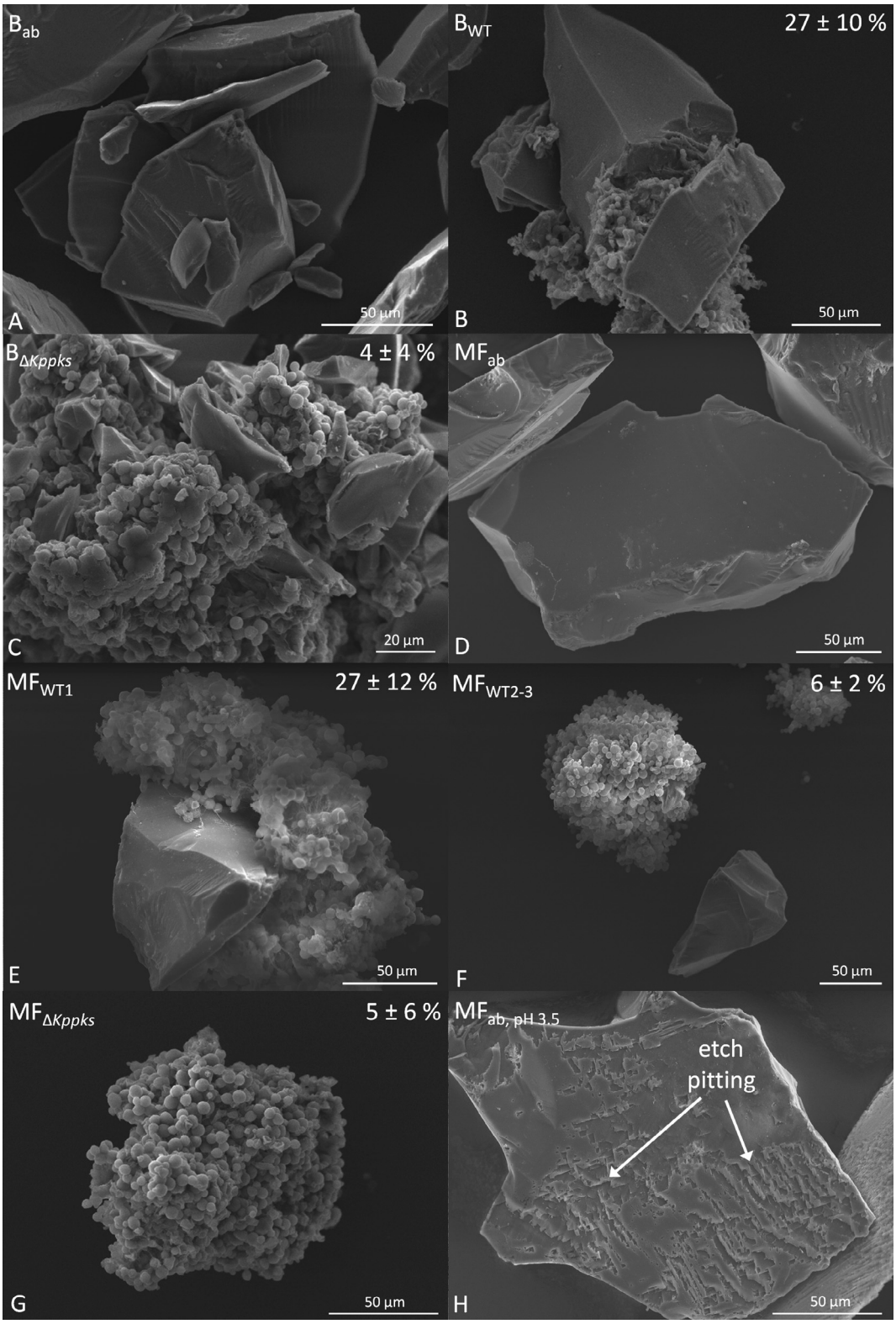

Fig. 5. The specific growth behaviour of the different *K. petricola* cultures and the etching patterns on the olivine shown by SEM imaging. The fungal aggregates of wild type runs B_{WT} (B) and MF_{WT1} (E) attached more to the olivine grains than the cultures of runs $MF_{WT2\text{-}3}$ (F) and *ΔKppks* runs $MF_{\Delta Kppks}$ (G). The surface of olivine grains from experiment $MF_{ab,pH\ 3.5}$ at pH 3.5 (H) was stronger etched than the surface of abiotic olivine grains at pH ~ 6 (A, D). The smaller olivine particles which are caught in the aggregate of *ΔKppks* cells (C) can also be seen on the abiotic olivine grains (A) and indicate that the olivine used in the batch experiments was not sufficiently cleaned before the experiment.

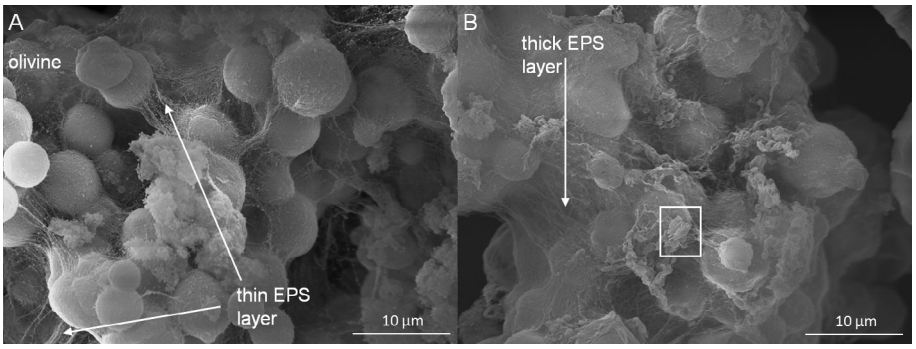

Fig. 6. The extracellular polymeric substances (EPS) of the wild type (A) and melanin-deficient mutant (B) of *K. petricola* shown by SEM imaging. The wild type produced a thin EPS layer (shown for MF_{WT1}, A). The mutant produces a thicker layer of EPS which covered the entire cell aggregates ($MF_{\Delta Kppks}$, B). Note the WT-EPS binding the olivine grains (A) and the small mineral precipitates seen in the case of $MF_{\Delta Kppks}$ (B, rectangle).

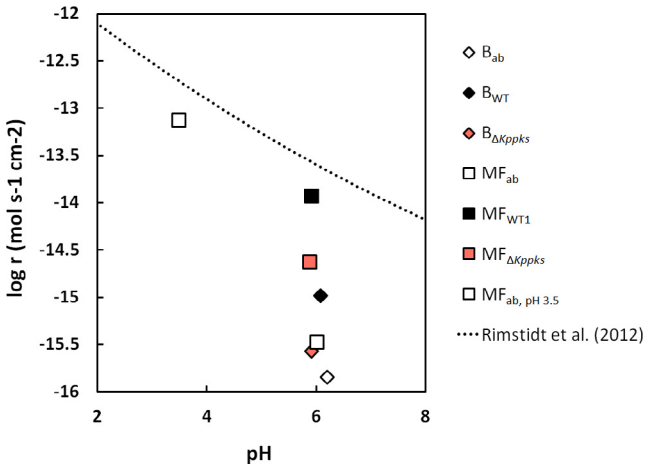

Fig. 7. Olivine dissolution rates from the abiotic and biotic batch (diamonds) and mixed flow (squares) experiments plotted as a function of pH and compared to literature data. The curve was calculated using equations reported by Rimstidt et al., (2012), which were based on literature data. Only the mixed flow WT (MF_{WT1}) and acidic abiotic ($MF_{ab,\ pH\ 3.5}$) runs had dissolution rates near the model from Rimstidt et al., (2012).

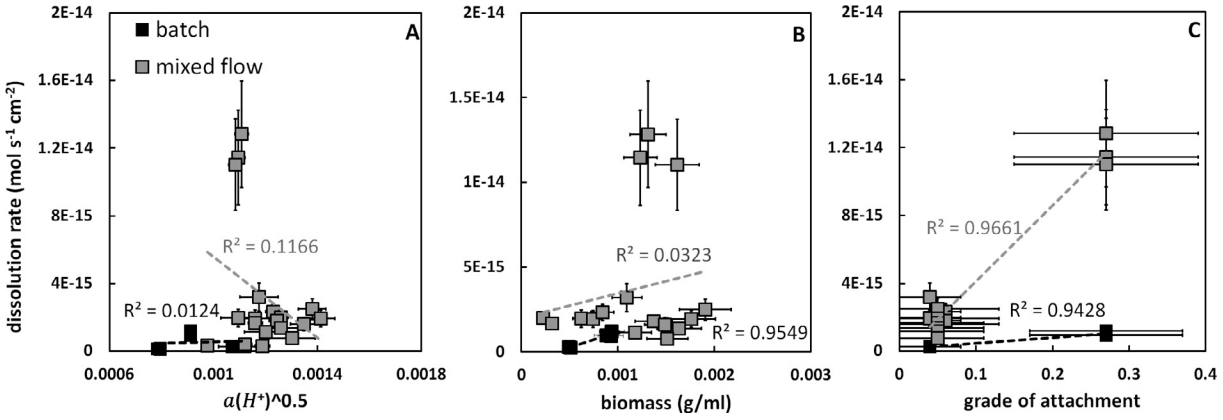

Fig. 8. The dependence of the olivine dissolution rate of each technical replicate on the respective (A) activity of protons to the power of 0.5 (i.e. $a_{H+}^{0.5}$), (B) biomass (mg/l) or (C) grade of attachment (%) grouped for batch and mixed flow experiments. The grade of attachment values are the means of the technical replicates. All error bars represent 2σ uncertainty (except for the biomass values: 1σ uncertainty) and are based on the (propagated) analytical uncertainty for the dissolution rate, $a_{H+}^{0.5}$ and biomass values. The error bars of the grade of attachment values are based on the standard deviation of the technical replicates. If error bars are not visible they are smaller than the symbol. The coefficient of determination (R^2) is shown for batch (in black) and mixed flow (in grey) experiments and was determined without taking the uncertainties into account.

atmosphere) and mixed flow (open to the atmosphere and continuous inflow of normally oxygenated solution) reactors used in this study ensures oxygenated conditions as shown by the absence of dissolved Fe in pH 6 runs. Other studies which did allow the oxidation of Fe(II), showed as well an inhibiting effect on olivine dissolution (Saldi et al., 2013; Torres et al., 2019). The exception being Sugimori et al. (2012), who showed that ferric hydroxide precipitation did not affect olivine dissolution by changing the partial pressure of atmospheric oxygen. In any case, we believe that a system like ours involving slow medium flow rates and reactors open to the atmosphere, approximates aerated Earth surface conditions more adequately and has merit.

The exact mechanism by which ferric Fe inhibits olivine dissolution is less known. Schott and Berner (1983; 1985) previously observed both the precipitation of a ferric hydroxide and the formation of a Fe(III)-containing silicate layer on reacted bronzite $\{(Mg, Fe)_2(SiO_3)_2\}$ and fayalite (Fe_2SiO_4). They claimed that only the latter was dissolution-inhibiting as it could not be removed by ultrasonic cleaning and that it was probably less reactive. A similar process was also suggested by Welch and Banfield (2002): the presence of ferric Fe at the surface of fayalite would inhibit dissolution by formation of the less reactive laihunite $\{(Fe(II),Mg)Fe(III)_2(SiO_4)_2\}$.

A potential silica-rich surface layer, which could have formed at the onset of dissolution due to preferential Mg release (Fig. 3A and B), cannot explain the strong inhibition of dissolution recorded in this study. The dissolution rate kept decreasing after day one, when stoichiometric dissolution had already been reached. In contrast, Fe kept being removed from solution throughout the entire duration of the experimental runs, suggesting that Fe(III) enrichment of the olivine surface exerted a much stronger influence than a potential silica layer. Furthermore, unlike in experiments like those of Daval et al. (2011), the solution in the reactors never attained equilibrium with regard to amorphous silica: our aqueous Si concentrations (Fig. 2D and E) remained well below the solubility of amorphous silica of 1.93 mM (Rimstidt and Barnes, 1980).

The influence of the nutrient components of the medium solution is as well negligible as was observed previously by Shirokova et al. (2012). The dissolution rates of experiments with MilliQ water ($B_{ab,\ MQ}$), with CNPS medium ($B_{ab,\ unbuffered}$) and with CNPS medium with the MES buffer ($B_{ab,\ buffered}$) were similar (Table D.1, Supplementary data 1).

4.2. Biotic olivine dissolution

Both the wild type and the melanin-deficient mutant in batch and mixed flow experiments enhanced olivine dissolution compared to the abiotic controls. The biotic dissolution rates did not keep decreasing and were higher than the abiotic rates, indicating a lower inhibition of olivine dissolution. The difference between the biotic and abiotic rates was generally larger for the mixed flow set-up than for the batch set-up. This can be explained by a continuous removal of solubilised Fe (Fig. 3E) out of the biotic mixed flow reactors ensuring olivine dissolution and preventing Fe (III) enrichment of the olivine surface. Also product inhibition and a limited nutrient supply, both of which slow down biological growth in batch reactors, are avoided in continuous, mixed flow reactors (Andric et al., 2010; Khamseh and Miccio, 2012; Picardo et al., 2013).

The biotic olivine dissolution rates diverged from the abiotic ones after 10 to 15 days of weathering, which correlates with the exponential growth phase of both the wild type and the mutant (growth experiment, Fig. D.1, Supplementary data 1). In general, various biological mechanisms could be involved in the observed fungal acceleration of olivine dissolution, cellular uptake of aqueous Fe being the most obvious. Based on the results from the metal binding experiment (Table 2), both the WT and Δ*Kppks* are theoretically able to sequester all Fe released by olivine dissolution. Fungi are as well capable of releasing a range of ligands which can complex metals and thereby increase the mineral dissolution rate (Wogelius and Walther, 1991; Drever and Stillings, 1997; Hoffland et al., 2004; Schmalenberger et al., 2015; Li et al., 2016). Most of interest to this study are siderophores, Fe-complexing ligands which *K. petricola* is able to produce (Favero-Longo et al., 2011). Comparison of the genome of *K. petricola* A95 to that of the filamentous fungus *Aspergillus fumigatus* revealed that *K. petricola* A95 produces the siderophore (hydro)ferricrocin. The release of such Fe-binding ligands could prevent Fe(III)-enrichment of the olivine surface. Torres et al. (2019) showed that siderophores accelerate olivine dissolution even when the pH is buffered.

The higher amount of aqueous Fe in the biotic runs compared to the abiotic runs (Fig. 3D and 3E) further indicate the production of Fe chelators like siderophores. Apart from bound to Fe-chelating compounds, aqueous Fe in these biotic runs could be present as ferrous Fe when conditions are sufficiently reducing (i.e. $E_h < 0.2$ V at pH 6). Both reactor types were open to the atmosphere (through sterile filters) which would create oxygenated conditions. Fungal respiration could, however, have caused an oxygen depletion and more reducing conditions in the bulk fluid as proposed previously for bacteria (Brantley et al., 2004). Also extracellular ferric reductases or extracellular non-protein ferric reductants could be released into the bulk solution (Vartivarian and Cowart, 1999; Gerwien et al., 2017). Both would reduce oxidised Fe, keeping it in solution.

Two more comments need to be made. One, the Mg content of the biomass (based on the metal binding experiment, Table 2) is not significant compared to the amount of Mg released from olivine at the end of either batch or mixed flow experiments. This means that the observed differences in dissolution rate between the wild type, mutant and abiotic control were not caused by cellular Mg binding. Two, *K. petricola* grows subaerially in nature while being submerged in our dissolution experiments. This might have created further phenotypic changes.

4.3. Fungal attachment explains biotic dissolution rates best

The rates of fungal-induced olivine dissolution were however not similar: olivine dissolution was faster in the

presence of the wild type than in the presence of the mutant in both batch and mixed flow reactors (Fig. 4A and B). Variations in the bulk solution pH and the amount of biomass could explain the different olivine dissolution rate in the presence of the wild type and mutant. The bulk solution pH, which can decrease due to respiration and organic acid production, has a reported effect on olivine dissolution to the power of 0.5 (i.e. the dissolution rate correlates with the activity of protons by $a_{H+}^{0.5}$) (Pokrovsky and Schott, 2000; Crundwell, 2014). Furthermore, a lower pH can slow down the oxidation of ferrous Fe (Singer and Stumm, 1970). Variations in biomass (Table 1) may as well have an impact as a higher biomass is associated with a higher binding of released Fe (Table 2). However, we did not detect a statistically significant correlation between the dissolution rates and either pH (R^2 of 0.012 and 0.12 for batch and mixed flow rates, respectively) or biomass (R^2 of 0.95 and 0.032 for batch and mixed flow rates, respectively) (see the method section for details on statistics and Fig. 8 for the plots).

Some WT mixed flow runs (i.e. MF_{WT2-3}) showed a lower grade of attachment and had dissolution rates comparable to those of the mutant runs (Fig. 4B). Therefore, a third parameter which may explain the dissolution rates is the *grade of attachment*, defined as the fraction of olivine grains colonised by fungi. Plotting the biotic olivine dissolution rate against its respective grade of attachment for each technical replicate results in a R^2 of 0.94 and 0.97 for batch and mixed flow, respectively (Fig. 8), indicating correlation. We can therefore conclude that the grade of attachment is the most predictive factor for the dissolution rates. The positive influence of fungal attachment to the mineral surface on mineral dissolution was previously shown by several studies (Li et al., 2009; Ahmed and Holmstrom, 2015; Li et al., 2016).

4.4. The cause of fungal attachment

Why does the wild type attach more to olivine than the melanin-deficient mutant? Apart from whether a mineral contains essential nutrients, attachment is also dependent on the chemistry of the EPS layer, the components of the cell wall and the chemistry of the solution (Lehrer et al., 1988; Caesartonthat and Epstein, 1991; Rogers and Bennett, 2004; Tourney and Ngwenya, 2014; Cai et al., 2018). Since the medium solution and the environmental conditions were the same in all conducted experiments, the origin of the different degrees of attachment is probably biological.

The melanin layer of the cell wall plays a role in metal adsorption and the turgor pressure, but is also hydrophobic and might thus increase adhesion (Pihet et al., 2009). However, WT runs which did not attach as well to the olivine were still black (i.e. produced melanin), indicating that melanin is not the cause of the attachment capacities of the WT.

The melanin-deficient mutant Δ*Kppks* produces more EPS than the wild type and its EPS has a different composition (Breitenbach, 2018). In *K. petricola* WT, pullulan constitutes the major part of the extracellular polysaccharide fraction (Breitenbach, 2018). This extracellular polysaccharide has an important function in the adhesion capacity of its eponymous fungus *Aureobasidium pullulans* (Bardage and Bjurman, 1998; Pouliot et al., 2005). The high attachment capacity of the wild type might thus be caused by its pullulan-rich EPS. Δ*Kppks*, on the other hand, forms less pullulan and more galactomannan (Breitenbach, 2018). Polymers similar to galactomannan have so far been described mainly in pathogenic, melanised fungi in which they are considered to be involved in virulence (Latge et al., 1994; Sassaki et al., 2011; Shibata and Okawa, 2011). A lower amount of the adhesive pullulan in the mutant may have prevented it from adhering to and interacting with the olivine surface. As variations in EPS composition are also possible without changes in the genetic background, the observed differences in the attachment capacity of the WT runs could be explained by a difference in EPS composition and have to be further studied in detail. To conclude, even though attachment is a complex process, there are indications that differences in the EPS composition play a major role in the attachment of *K. petricola* to olivine.

4.5. How fungal attachment prevents the inhibition of olivine dissolution

Various biological mechanisms could explain how fungal attachment further prevents the inhibitory effects of Fe(II) oxidation at the surface. Starting with the production of Fe chelators like siderophores: Ahmed and Holmstrom (2015) observed that fungal siderophore production increased following attachment to biotite $\{K(Mg, Fe)_3AlSi_3O_{10}(F,OH)_2\}$. A similar mechanism might be at work in our experiments. Another option is the reuse of the Fe chelator by cell surface ferric reductases, of which encoding genes are present in the genome of *K. petricola* A95. This reductase is part of the reductive Fe assimilation system: it reduces chelator-complexed ferric Fe to ferrous Fe which is then taken up by the cell (Philpott, 2006; Haas et al., 2008). The now Fe-free chelator can be reused to transport more Fe to the reductase. Biofilm formation enhances the use efficiency of Fe chelators as the distance between cell surface reductase and Fe source is reduced (Rizzi et al., 2019). Chelators of an unattached cell would have to diffuse much longer distances between the reductase and the olivine surface. Interestingly the product of this enzymatic reaction, ferrous Fe, is thought to bind to melanin, making it capable to neutralise antifungal oxidants (Jacobson and Hong, 1997). The melanin-deficient mutant would not be able to bind this ferrous Fe, another possible cause of its higher aqueous Fe/Si ratios (Fig. 3D and E). Another possible scenario follows from the observation from Torres et al. (2019); they showed that only substantial (>100 μM) siderophore concentrations impact olivine dissolution. Such high concentrations aren't likely to be reached in the bulk solution. Aqueous Fe concentrations, an indicator of the production of Fe chelators, are around 1 μM (Fig. 2G and H). Higher chelator concentrations could however be reached within the biofilm, at the mineral surface, again explaining the importance of fungal attachment to olivine

dissolution. Fe could as well have precipitated in the EPS as ferric hydroxides (Welch and Banfield, 2002; Yu et al., 2016). This, as proposed by Rizzi et al. (2019), might prevent further condensation of ferric hydroxides, helping chelators to scavenge Fe. Apart from Fe chelator production, O_2 uptake through fungal respiration may create a local reduced environment around the cells, inhibiting Fe oxidation at the olivine surface. This effect would as well be stronger upon attachment. An enhancement in the production of organic acids is unlikely as these compounds have never been observed for *K. petricola* or any rock-inhabiting fungus (Gorbushina et al., 1993; Selbmann et al., 2005; Marvasi et al., 2012).

Fungal attachment might also be associated with a locally reduced pH at the biofilm-olivine interface, thus enhancing olivine dissolution. The acidification experiment shows that both the wild type and the mutant are able to reduce the bulk pH of unbuffered medium to ca. 3 (Fig. D.2, Supplementary data 1). This was most likely caused by fungal respiration (i.e. production of CO_2) as organic acid production has never been observed for *K. petricola* or any rock-inhabiting fungus (Gorbushina et al., 1993; Selbmann et al., 2005; Marvasi et al., 2012). A local decrease of the pH could impact the dissolution rate directly by metal-proton exchange reactions or indirectly through the reduction of the Fe(II) oxidation rate which prevents Fe(III) oxyhydroxide precipitation and the Fe (III) adsorption at the mineral surface (Singer and Stumm, 1970; Morgan and Lahav, 2007; Oelkers et al., 2018). However, results of a study with bacteria contradict this hypothesis: the pH inside the biofilm is only marginally lower when the pH of the nutrient solution is buffered (Liermann et al., 2000). Moreover, etching on the biotically-reacted olivine surface at pH 6 was observed only once and without connection to cell aggregates. The abiotically-reacted olivine surface at pH 3.5 was nevertheless strongly etched (Fig. 5H). All this indicates that a local pH effect is unlikely the major cause of the higher biotic olivine dissolution rates.

Knocking-out the gene *KpPKS* might have altered the potential production of weathering-affecting compounds like siderophores, Fe reductases, organic acids or superoxides as it did for the composition of EPS. This might explain the observed differences in fungal olivine dissolution rates but would only apply if these alterations would correlate with the grade of attachment.

To conclude, the WT in run MF_{WT1} was able to prevent the inhibition of olivine dissolution to the point that its dissolution rate (log r of −13.9) approached the abiotic rates previously published (log r of −13.1) (reviewed by Rimstidt et al. (2012), Fig. 7). This is mainly due to the strong reduction of the inhibiting effect of ferrous Fe oxidation, but secondary effects like pH reduction and other complexation reactions may also play a role. Allowing olivine-released Fe to oxidise resulted in olivine dissolution rates that are more relevant to natural processes. Our abiotic dissolution rates are similar to those from a microcosm experiment by Renforth et al. (2015), thus showing that the mixed flow set-up offers reliable conditions for conducting geomicrobiological research. We believe that these findings could be generally applied to the chemical weathering of all Fe(II)-bearing silicate minerals like olivines, pyroxenes, hornblende, biotite, etc., whose dissolution is inhibited by Fe oxidation (Schott and Berner, 1983; Schott and Berner, 1985; Santelli et al., 2001; Golubev et al., 2005; Ahmed and Holmstrom, 2015). The effect of iron oxidation on the reported olivine dissolution rates makes these findings specifically relevant to chemical weathering under aerobic conditions as found in subaerial biofilms or unsaturated soils (Scott, 1955; Neale et al., 2000). And finally, Fe is a vital nutrient for all forms of life; bacteria and fungi alike are known to oxidise, reduce and sequester Fe (Delatorre and Gomezalarcon, 1994; Philpott, 2006; Melton et al., 2014). The conditions under which one of these microbial mechanisms gains the upper hand in mineral weathering should be explored in future studies. In experiments with genetically tractable microorganisms, the role of these different microbial traits can be singled out to facilitate our understanding of bio-weathering processes.

5. CONCLUSION

Here we have shown that abiotic dissolution of olivine under oxygenated conditions and low flow rates is strongly inhibited at pH 6 but not at pH 3.5. Chemical analyses of the reacting fluid and XPS analyses of the olivine surface indicate that *in-situ* oxidation of ferrous Fe and/or ferric hydroxide precipitation at the olivine surface lowers olivine's reactivity, causing the inhibition. This inhibition of olivine dissolution is not as pronounced in the presence of the wild type of the rock-inhabiting fungus *K. petricola* and its melanin-deficient mutant Δ*Kppks*. Both were able to sequester important quantities of Fe and retain Fe in solution, most likely by production of Fe chelators like siderophores. Each process prevents *in-situ* ferrous Fe oxidation and the inhibition of olivine dissolution. The fungal impact on olivine dissolution was not only larger in mixed flow reactors, but also when wild type cells were firmly attached to the olivine surface. Once fungi were attached, olivine dissolution was no longer inhibited. This is possibly caused by a higher reuse of Fe chelators within the biofilm of attached fungi, preventing the Fe(III)-enrichment of the olivine surface. The fungal attachment capacity is probably linked to the production of pullulan-rich EPS. To conclude, our long term, biologically and geochemically controlled mixed flow experiments allow the oxidation of ferrous Fe and stable growth of rock-inhabiting fungi, thus establishing dissolution rates more relevant to olivine weathering at Earth surface conditions.

Declaration of Competing Interest

The authors declare that they have no known competing financial interests or personal relationships that could have appeared to influence the work reported in this paper.

ACKNOWLEDGEMENT

We would like to thank Nicole Knabe and Oliver Voigt for the creation of the knock-out mutant Δ*Kppks*, Ralf Milke for micro-

probe analysis, Carsten Prinz and Annett Zimathies for the BET analysis, Julia Schumacher and Felix Heeger for gene expression analysis and finally Oleg Pokrovsky and Jörg Toepel for advice on the experimental design. This study was supported financially by a grant from the People Programme (Marie Curie Actions) of the European Union's Seventh Framework Programme FP7/2007-2013/under REA grant agreement no. 608069 in the framework of the ISONOSE Marie Curie initial training network and by internal funds of the BAM. We also thank the three anonymous reviewers, whose comments significantly improved the manuscript.

APPENDIX A. SUPPLEMENTARY DATA

Supplementary data to this article can be found online at https://doi.org/10.1016/j.gca.2020.05.010.

REFERENCES

Abdulla H. (2009) Bioweathering and Biotransformation of Granitic Rock Minerals by Actinomycetes. *Microb. Ecol.* **58**, 753–761.

Adeyemi A. O. and Gadd G. M. (2005) Fungal degradation of calcium-, lead- and silicon-bearing minerals. *Biometals* **18**, 269–281.

Ahmadjian V. and Hale M. E. (1973) *The lichens*. Academic Press, New York.

Ahmed E. and Holmstrom S. J. M. (2015) Microbe-mineral interactions: The impact of surface attachment on mineral weathering and element selectivity by microorganisms. *Chem. Geol.* **403**, 13–23.

Andric P., Meyer A. S., Jensen P. A. and Dam-Johansen K. (2010) Reactor design for minimizing product inhibition during enzymatic lignocellulose hydrolysis: I. Significance and mechanism of cellobiose and glucose inhibition on cellulolytic enzymes. *Biotechnol. Adv.* **28**, 308–324.

Banfield J. F., Barker W. W., Welch S. A. and Taunton A. (1999) Biological impact on mineral dissolution: Application of the lichen model to understanding mineral weathering in the rhizosphere. *P. Natl. Acad. Sci. USA* **96**, 3404–3411.

Bardage S. L. and Bjurman J. (1998) Isolation of an Aureobasidium pullulans polysaccharide that promotes adhesion of blastospores to water-borne paints. *Can. J. Microbiol.* **44**, 954–958.

Biesinger M. C., Payne B. P., Grosvenor A. P., Lau L. W. M., Gerson A. R. and Smart R. S. (2011) Resolving surface chemical states in XPS analysis of first row transition metals, oxides and hydroxides: Cr, Mn, Fe, Co and Ni. *Appl. Surf. Sci.* **257**, 2717–2730.

Bonneville S., Bray A. W. and Benning L. G. (2016) Structural Fe (II) Oxidation in Biotite by an Ectomycorrhizal Fungi Drives Mechanical Forcing. *Environ. Sci. Technol.* **50**, 5589–5596.

Bonneville S., Smits M. M., Brown A., Harrington J., Leake J. R., Brydson R. and Benning L. G. (2009) Plant-driven fungal weathering: Early stages of mineral alteration at the nanometer scale. *Geology* **37**, 615–618.

Brantley S. L., Liermann L. J., Guynn R. L., Anbar A., Icopini G. A. and Barling J. (2004) Fe isotopic fractionation during mineral dissolution with and without bacteria. *Geochim. Cosmochim. Ac* **68**, 3189–3204.

Breitenbach R. (2018) *Biochemische und physiologische Charakterisierung der extrazellulären Matrix eines Modellbiofilms*. Freie Universität Berlin, BCP.

Breitenbach R., Silbernagl D., Toepel J., Sturm H., Broughton W. J., Sassaki G. L. and Gorbushina A. A. (2018) Corrosive extracellular polysaccharides of the rock-inhabiting model fungus Knufia petricola. *Extremophiles* **22**, 165–175.

Bundeleva I. A., Menez B., Auge T., Bodenan F., Recham N. and Guyot F. (2014) Effect of cyanobacteria Synechococcus PCC 7942 on carbonation kinetics of olivine at 20 degrees C. *Miner. Eng.* **59**, 2–11.

Caesartonthat T. C. and Epstein L. (1991) Adhesion-Reduced Mutants and the Wild-Type Nectria-Haematococca - an Ultrastructural Comparison of the Macroconidial Walls. *Exp. Mycol.* **15**, 193–205.

Cai L., Xiao H. R., Huang S. M., Li H. and Zhou G. T. (2013) Solubilization of Magnesium-Bearing Silicate Minerals and the Subsequent Formation of Glushinskite by Aspergillus niger. *Geomicrobiol. J.* **30**, 302–312.

Cai P., Lin D., Peacock C. L., Peng W. X. and Huang Q. Y. (2018) EPS adsorption to goethite: Molecular level adsorption mechanisms using 2D correlation spectroscopy. *Chem. Geol.* **494**, 127–135.

Carlson T. A. (1975) *Photoelectron and Auger spectroscopy*. Plenum Press, New York.

Chen J., Blume H. P. and Beyer L. (2000) Weathering of rocks induced by lichen colonization - a review. *Catena* **39**, 121–146.

Crundwell F. K. (2014) The mechanism of dissolution of forsterite, olivine and minerals of the orthosilicate group. *Hydrometallurgy* **150**, 68–82.

Daval D., Sissmann O., Menguy N., Saldi G. D., Guyot F., Martinez I., Corvisier J., Garcia B., Machouk I., Knauss K. G. and Hellmann R. (2011) Influence of amorphous silica layer formation on the dissolution rate of olivine at 90 degrees C and elevated pCO(2). *Chem. Geol.* **284**, 193–209.

Delatorre M. A. and Gomezalarcon G. (1994) Manganese and iron oxidation by fungi isolated from building stone. *Microb. Ecol.* **27**, 177–188.

Drever J. I. and Stillings L. L. (1997) The role of organic acids in mineral weathering. *Colloids Surf. a-Physicochem. Eng. Aspects* **120**, 167–181.

Duane M. J. (2006) Coeval biochemical and biophysical weathering processes on Quaternary sandstone terraces south of Rabat (Temara), northwest Morocco. *Earth Surf. Proc. Land.* **31**, 1115–1128.

Dunne W. M. (2002) Bacterial adhesion: Seen any good biofilms lately?. *Clin. Microbiol. Rev.* **15** 155-+.

Favero-Longo S. E., Gazzano C., Girlanda M., Castelli D., Tretiach M., Baiocchi C. and Piervittori R. (2011) Physical and Chemical Deterioration of Silicate and Carbonate Rocks by Meristematic Microcolonial Fungi and Endolithic Lichens (Chaetothyriomycetidae). *Geomicrobiol. J.* **28**, 732–744.

Fernandez C. W. and Koide R. T. (2013) The function of melanin in the ectomycorrhizal fungus Cenococcum geophilum under water stress. *Fungal Ecol.* **6**, 479–486.

Flemming H. C., Wingender J., Szewzyk U., Steinberg P., Rice S. A. and Kjelleberg S. (2016) Biofilms: an emergent form of bacterial life. *Nat. Rev. Microbiol.* **14**, 563–575.

Fogarty R. V. and Tobin J. M. (1996) Fungal melanins and their interactions with metals. *Enzyme Microb. Tech.* **19**, 311–317.

Gadd G. M. (2007) Geomycology: biogeochemical transformations of rocks, minerals, metals and radionuclides by fungi, bioweathering and bioremediation. *Mycol. Res.* **111**, 3–49.

Gadd G. M. and Derome L. (1988) Biosorption of Copper by Fungal Melanin. *Appl. Microbiol. Biotechnol.* **29**, 610–617.

Garcia B., Lemelle L., Rose-Koga E., Perriat P., Basset R., Gillet P. and Albarede F. (2013) An experimental model approach of biologically-assisted silicate dissolution with olivine and Escherichia coli - Impact on chemical weathering of mafic rocks and atmospheric CO2 drawdown. *Appl. Geochem.* **31**, 216–227.

Gerwien F., Safyan A., Wisgott S., Brunke S., Kasper L. and Hube B. (2017) The Fungal Pathogen Candida glabrata Does Not Depend on Surface Ferric Reductases for Iron Acquisition. *Front. Microbiol.* **8**.

Golubev S. V., Pokrovsky O. S. and Schott J. (2005) Experimental determination of the effect of dissolved CO2 on the dissolution kinetics of Mg and Ca silicates at 25 degrees C. *Chem. Geol.* **217**, 227–238.

Gorbushina A. A. (2007) Life on the rocks. *Environ. Microbiol.* **9**, 1613–1631.

Gorbushina A. A., Kotlova E. R. and Sherstneva O. A. (2008) Cellular responses of microcolonial rock fungi to long-term desiccation and subsequent rehydration. *Stud. Mycol.*, 91–97.

Gorbushina A. A., Krumbein W. E., Hamman C. H., Panina L., Soukharjevski S. and Wollenzien U. (1993) Role of Black Fungi in Color-Change and Biodeterioration of Antique Marbles. *Geomicrobiol. J.* **11**, 205–221.

Goriely A. and Tabor M. (2006) Estimates of biomechanical forces in Magnaporthe grisea. *Mycol. Res.* **110**, 755–759.

Haas H., Eisendle M. and Turgeon B. G. (2008) Siderophores in fungal physiology and virulence. *Annu. Rev. Phytopathol.* **46**, 149–187.

Hanchen M., Prigiobbe V., Storti G., Seward T. M. and Mazzotti M. (2006) Dissolution kinetics of fosteritic olivine at 90–150 degrees C including effects of the presence of CO2. *Geochim. Cosmochim. Ac* **70**, 4403–4416.

Hauer T., Muhlsteinova R., Bohunicka M., Kastovsky J. and Mares J. (2015) Diversity of cyanobacteria on rock surfaces. *Biodivers. Conserv.* **24**, 759–779.

Hochella M. F. and Carim A. H. (1988) A Reassessment of Electron-Escape Depths in Silicon and Thermally Grown Silicon Dioxide Thin-Films. *Surf. Sci.* **197**, L260–L268.

Hoffland E., Kuyper T. W., Wallander H., Plassard C., Gorbushina A. A., Haselwandter K., Holmstrom S., Landeweert R., Lundstrom U. S., Rosling A., Sen R., Smits M. M., van Hees P. A. and van Breemen N. (2004) The role of fungi in weathering. *Front. Ecol. Environ.* **2**, 258–264.

Howard R. J. and Ferrari M. A. (1989) Role of Melanin in Appressorium Function. *Exp. Mycol.* **13**, 403–418.

Howard R. J., Ferrari M. A., Roach D. H. and Money N. P. (1991) Penetration of Hard Substrates by a Fungus Employing Enormous Turgor Pressures. *P. Natl. Acad. Sci. USA* **88**, 11281–11284.

Jacobson E. S. and Hong J. D. (1997) Redox buffering by melanin and Fe(II) in Cryptococcus neoformans. *J. Bacteriol.* **179**, 5340–5346.

Khamseh A. A. G. and Miccio M. (2012) Comparison of batch, fed-batch and continuous well-mixed reactors for enzymatic hydrolysis of orange peel wastes. *Process Biochem.* **47**, 1588–1594.

Knabe N., Breitenbach R., Dementyeva P., Heeger F., Mazzoni C. and Gorbushina A. A. (2017) *Some like it on the rocks: recurring stresses select for rock-inhabiting fungi with manifold protective pigments, 27th Fungal Genetics Conference Asilomar*. Pacific Grove, USA.

Kohler P., Hartmann J. and Wolf-Gladrow D. A. (2010) Geoengineering potential of artificially enhanced silicate weathering of olivine. *Proc. Natl. Acad. Sci. USA* **107**, 20228–20233.

Krumbein W. E. and Jens K. (1981) Biogenic Rock Varnishes of the Negev Desert (Israel) an Ecological Study of Iron and Manganese Transformation by Cyanobacteria and Fungi. *Oecologia* **50**, 25–38.

Latge J. P., Kobayashi H., Debeaupuis J. P., Diaquin M., Sarfati J., Wieruszeski J. M., Parra E., Bouchara J. P. and Fournet B. (1994) Chemical and Immunological Characterization of the Extracellular Galactomannan of Aspergillus-Fumigatus. *Infect. Immun.* **62**, 5424–5433.

Lehrer N., Segal E., Lis H. and Gov Y. (1988) Effect of Candida-Albicans Cell-Wall Components on the Adhesion of the Fungus to Human and Murine Vaginal Mucosa. *Mycopathologia* **102**, 115–121.

Li W., Zhou P. P., Jia L. P., Yu L. J., Li X. L. and Zhu M. (2009) Limestone Dissolution Induced by Fungal Mycelia, Acidic Materials, and Carbonic Anhydrase from Fungi. *Mycopathologia* **167**, 37–46.

Li Z. B., Liu L. W., Chen J. and Teng H. H. (2016) Cellular dissolution at hypha- and spore-mineral interfaces revealing unrecognized mechanisms and scales of fungal weathering. *Geology* **44**, 319–322.

Liermann L. J., Barnes A. S., Kalinowski B. E., Zhou X. Y. and Susan L. (2000) Microenvironments of pH in biofilms grown on dissolving silicate surfaces. *Chem. Geol.* **171**, 1–16.

Linder M. B., Szilvay G. R., Nakari-Setala T. and Penttila M. E. (2005) Hydrophobins: the protein-amphiphiles of filamentous fungi. *FEMS Microbiol. Rev.* **29**, 877–896.

Luce R. W., Bartlett R. W. and Parks G. A. (1972) Dissolution Kinetics of Magnesium Silicates. *Geochim. Cosmochim. Ac* **36**, 35-&.

Maher K., Johnson N. C., Jackson A., Lammers L. N., Torchinsky A. B., Weaver K. L., Bird D. K. and Brown G. E. (2016) A spatially resolved surface kinetic model for forsterite dissolution. *Geochim. Cosmochim. Ac* **174**, 313–334.

Martinez R. E., Weber S. and Bucher K. (2014) Quantifying the kinetics of olivine dissolution in partially closed and closed batch reactor systems. *Chem. Geol.* **367**, 1–12.

Marvasi M., Donnarumma F., Frandi A., Mastromei G., Sterflinger K., Tiano P. and Perito B. (2012) Black microcolonial fungi as deteriogens of two famous marble statues in Florence, Italy. *Int. Biodeter. Biodegr.* **68**, 36–44.

Melton E. D., Swanner E. D., Behrens S., Schmidt C. and Kappler A. (2014) The interplay of microbially mediated and abiotic reactions in the biogeochemical Fe cycle. *Nat. Rev. Microbiol.* **12**, 797–808.

Millero F. J. (1985) The Effect of Ionic Interactions on the Oxidation of Metals in Natural-Waters. *Geochim Cosmochim Ac* **49**, 547–553.

Money N. P. and Howard R. J. (1996) Confirmation of a link between fungal pigmentation, turgor pressure, and pathogenicity using a new method of turgor measurement. *Fungal Genet. Biol.* **20**, 217–227.

Morgan B. and Lahav O. (2007) The effect of pH on the kinetics of spontaneous Fe(II) oxidation by O-2 in aqueous solution - basic principles and a simple heuristic description. *Chemosphere* **68**, 2080–2084.

Nai C., Wong H. Y., Pannenbecker A., Broughton W. J., Benoit I., de Vries R. P., Gueidan C. and Gorbushina A. A. (2013) Nutritional physiology of a rock-inhabiting, model microcolonial fungus from an ancestral lineage of the Chaetothyriales (Ascomycetes). *Fungal Genet. Biol.* **56**, 54–66.

Nakari-Setala T., Azeredo J., Henriques M., Oliveira R., Teixeira J., Linder M. and Penttila M. (2002) Expression of a fungal hydrophobin in the Saccharomyces cerevisiae cell wall: Effect on cell surface properties and immobilization. *Appl. Environ. Microb.* **68**, 3385–3391.

Neale C. N., Hughes J. B. and Ward C. H. (2000) Impacts of unsaturated zone properties on oxygen transport and aquifer reaeration. *Ground Water* **38**, 784–794.

Oelkers E. H. (2001) An experimental study of forsterite dissolution rates as a function of temperature and aqueous Mg and Si concentrations. *Chem. Geol.* **175**, 485–494.

Oelkers E. H., Benning L. G., Lutz S., Mavromatis V., Pearce C. R. and Plumper O. (2015) The efficient long-term inhibition of forsterite dissolution by common soil bacteria and fungi at Earth surface conditions. *Geochim. Cosmochim. Ac* **168**, 222–235.

Oelkers E. H., Declercq J., Saldi G. D., Gislason S. R. and Schott J. (2018) Olivine dissolution rates: A critical review. *Chem. Geol.* **500**, 1–19.

Olsen A. A., Hausrath E. M. and Rimstidt J. D. (2015) Forsterite dissolution rates in Mg-sulfate-rich Mars-analog brines and implications of the aqueous history of Mars. *J. Geophys. Res.-Planet* **120**, 388–400.

Paolo W. F., Dadachova E., Mandal P., Casadevall A., Szaniszlo P. J. and Nosanchuk J. D. (2006) Effects of disrupting the polyketide synthase gene WdPKS1 in Wangiella [Exophiala] dermatitidis on melanin production and resistance to killing by antifungal compounds, enzymatic degradation, and extremes in temperature. *BMC Microbiol.* **6**.

Philpott C. C. (2006) Iron uptake in fungi: A system for every source. *Bba-Mol. Cell Res.* **1763**, 636–645.

Picardo M. C., de Medeiros J. L., Araujo O. D. F. and Chaloub R. M. (2013) Effects of CO2 enrichment and nutrients supply intermittency on batch cultures of Isochrysis galbana. *Bioresource Technol* **143**, 242–250.

Pihet M., Vandeputte P., Tronchin G., Renier G., Saulnier P., Georgeault S., Mallet R., Chabasse D., Symoens F. and Bouchara J. P. (2009) Melanin is an essential component for the integrity of the cell wall of Aspergillus fumigatus conidia. *BMC Microbiol.* **9**.

Pokrovsky O. S. and Schott J. (2000) Kinetics and mechanism of forsterite dissolution at 25 degrees C and pH from 1 to 12. *Geochim. Cosmochim. Ac* **64**, 3313–3325.

Pouliot J. M., Walton I., Parkhouse M. N., Abu-Lail L. I. and Camesano T. A. (2005) Adhesion of Aureobasidium pullulans is controlled by uronic acid based polymers and pullulan. *Biomacromolecules* **6**, 1122–1131.

Reed S. J. B. (2005) *Electron microprobe analysis and scanning electron microscopy in geology*, 2nd ed. Cambridge University Press, Cambridge.

Renforth P., von Strandmann P. A. E. P. and Henderson G. M. (2015) The dissolution of olivine added to soil: Implications for enhanced weathering. *Appl. Geochem.* **61**, 109–118.

Rimstidt J. D. and Barnes H. L. (1980) The Kinetics of Silica-Water Reactions. *Geochim. Cosmochim. Ac* **44**, 1683–1699.

Rimstidt J. D., Brantley S. L. and Olsen A. A. (2012) Systematic review of forsterite dissolution rate data. *Geochim. Cosmochim. Ac* **99**, 159–178.

Rippka R., Deruelles J., Waterbury J. B., Herdman M. and Stanier R. Y. (1979) Generic Assignments, Strain Histories and Properties of Pure Cultures of Cyanobacteria. *J. Gen. Microbiol.* **111**, 1–61.

Rizzi A., Roy S., Bellenger J. P. and Beauregard P. B. (2019) Iron Homeostasis in Bacillus subtilis Requires Siderophore Production and Biofilm Formation. *Appl. Environ. Microb.* **85**.

Roberts J. A. (2004) Inhibition and enhancement of microbial surface colonization: the role of silicate composition. *Chem. Geol.* **212**, 313–327.

Rogers J. R. and Bennett P. C. (2004) Mineral stimulation of subsurface microorganisms: release of limiting nutrients from silicates. *Chem. Geol.* **203**, 91–108.

Rosso J. J. and Rimstidt J. D. (2000) A high resolution study of forsterite dissolution rates. *Geochim. Cosmochim. Ac* **64**, 797–811.

Saldi G. D., Daval D., Morvan G. and Knauss K. G. (2013) The role of Fe and redox conditions in olivine carbonation rates: An experimental study of the rate limiting reactions at 90 and 150 degrees C in open and closed systems. *Geochim. Cosmochim. Ac* **118**, 157–183.

Santelli C. M., Welch S. A., Westrich H. R. and Banfield J. F. (2001) The effect of Fe-oxidizing bacteria on Fe-silicate mineral dissolution. *Chem. Geol.* **180**, 99–115.

Sassaki G. L., Czelusniak P. A., Vicente V. A., Zanata S. M., Souza L. M., Gorin P. A. J. and Iacomini M. (2011) Some biomolecules and a partially O-acetylated exo-galactomannan containing beta-Galf units from pathogenic Exophiala jeanselmei, having a pronounced immunogenic response. *Int. J. Biol. Macromol.* **48**, 177–182.

Schmalenberger A., Duran A. L., Bray A. W., Bridge J., Bonneville S., Benning L. G., Romero-Gonzalez M. E., Leake J. R. and Banwart S. A. (2015) Oxalate secretion by ectomycorrhizal Paxillus involutus is mineral-specific and controls calcium weathering from minerals. *Sci. Rep.-Uk*, 5.

Schott J. and Berner R. A. (1983) X-Ray Photoelectron Studies of the Mechanism of Iron Silicate Dissolution during Weathering. *Geochim. Cosmochim. Ac* **47**, 2233–2240.

Schott J. and Berner R. A. (1985) Dissolution Mechanisms of Pyroxenes and Olivines During Weathering. *Chem. Weather.*, 35–53.

Schuessler J. A., Kampf H., Koch U. and Alawi M. (2016) Earthquake impact on iron isotope signatures recorded in mineral spring water. *J. Geophys. Res.-Sol. Ea* **121**, 8548–8568.

Schuiling R. D. and Krijgsman P. (2006) Enhanced weathering: An effective and cheap tool to sequester CO2. *Clim. Change* **74**, 349–354.

Scott, A.D. and.Evans, D.D., Dissolved oxygen in saturated soil. *Soil Sci. Soc. Am. J.* **19**, 1955, 7-12.

Seiffert F., Bandow N., Bouchez J., von Blanckenburg F. and Gorbushina A. A. (2014) Microbial colonization of bare rocks: laboratory biofilm enhances mineral weathering. *Proced. Earth Plan Sc.* **10**, 123–129.

Selbmann L., de Hoog G. S., Mazzaglia A., Friedmann E. I. and Onofri S. (2005) Fungi at the edge of life: cryptoendolithic black fungi from Antarctic desert. *Stud. Mycol.*, 1–32.

Seyama H. and Soma M. (1987) Fe 2p Spectra of Silicate Minerals. *J. Electron. Spectrosc.* **42**, 97–101.

Shibata N. and Okawa Y. (2011) Chemical structure of beta-galactofuranose-containing polysaccharide and O-linked oligosaccharides obtained from the cell wall of pathogenic dematiaceous fungus Fonsecaea pedrosoi. *Glycobiology* **21**, 69–81.

Shirokova L. S., Benezeth P., Pokrovsky O. S., Gerard E., Menez B. and Alfredsson H. (2012) Effect of the heterotrophic bacterium Pseudomonas reactans on olivine dissolution kinetics and implications for CO2 storage in basalts. *Geochim. Cosmochim. Ac* **80**, 30–50.

Siegel S. M., Galun M. and Siegel B. Z. (1990) Filamentous Fungi as Metal Biosorbents - a Review. *Water Air Soil Poll.* **53**, 335–344.

Singer P. C. and Stumm W. (1970) Acidic Mine Drainage. Rate-Determining Step. *Science* **167**, 1121–2000.

Spurr A. R. (1969) A Low-Viscosity Epoxy Resin Embedding Medium for Electron Microscopy. *J. Ultrastruct. Res.* **26**, 31-&.

International Organization of Standardization, 2014. Determination of the specific surface area of solids by gas adsorption - BET method, DIN ISO 9277, Berlin.

Sugimori H., Kanzaki Y. and Murakami T. (2012) Relationships between Fe redistribution and Po-2 during mineral dissolution under low O-2 conditions. *Geochim. Cosmochim. Ac* **84**, 29–46.

Torres M. A., Dong S., Nealson K. H. and West A. J. (2019) The kinetics of siderophore-mediated olivine dissolution. *Geobiology* **17**, 401–416.

Tourney J. and Ngwenya B. T. (2014) The role of bacterial extracellular polymeric substances in geomicrobiology. *Chem. Geol.* **386**, 115–132.

Vartivarian S. E. and Cowart R. E. (1999) Extracellular iron reductases: Identification of a new class of enzymes by siderophore-producing microorganisms. *Arch. Biochem. Biophys.* **364**, 75–82.

von Blanckenburg F., Wittmann H. and Schuessler J. A. (2016) HELGES: Helmholtz Laboratory for the Geochemistry of the Earth Surface. *J. Large-scale Res. Facilit.*, 2.

Warscheid T. and Braams J. (2000) Biodeterioration of stone: a review. *Int. Biodeter. Biodegr.* **46**, 343–368.

Welch S. A. and Banfield J. F. (2002) Modification of olivine surface morphology and reactivity by microbial activity during chemical weathering. *Geochim. Cosmochim. Ac* **66**, 213–221.

Wessels J. G. H. (1996) Fungal hydrophobins: Proteins that function at an interface. *Trends Plant Sci.* **1**, 9–15.

Wogelius R. A. and Walther J. V. (1991) Olivine Dissolution at 25-Degrees-C - Effects of Ph, Co2, and Organic-Acids. *Geochim. Cosmochim. Ac* **55**, 943–954.

Yu S., Wei Q., Zhao T. H., Guo Y. and Ma L. Y. Z. (2016) A Survival Strategy for Pseudomonas aeruginosa That Uses Exopolysaccharides To Sequester and Store Iron To Stimulate Psl-Dependent Biofilm Formation. *Appl. Environ. Microb.* **82**, 6403–6413.

Associate editor: Owen Duckworth